Systematic detection of anomalous ionospheric perturbations above LEOs from GNSS POD data including possible tsunami signatures

Heng Yang, Manuel Hernández-Pajares, Wojciech Jarmołowski, Paweł Wielgosz, Sharon L. Vadas, Oscar L. Colombo, Enric Monte-Moreno, Alberto Garcia-Rigo, Victoria Graffigna, Anna Krypiak-Gregorczyk, Beata Milanowska, Pau Bofill-Soliguer, Germán Olivares-Pulido, Qi Liu, Roger Haagmans

***Abstract*—In this paper we show the capability of Global Navigation Satellite System (GNSS) Precise Orbit Determination (POD) Low Earth Orbiter (LEO) data to detect anomalous ionospheric disturbances in the spectral range of the signals associated to earthquakes and tsunamis, applied to two of these events in Papua New Guinea (PNG) and Solomon Islands during 2016. This is achieved thanks to the new PIES approach (*POD-GNSS LEO Detrended Ionospheric Electron Content Significant Deviations*). The significance of such ionospheric signals above the Swarm LEOs is confirmed with different types of independent data: in-situ electron density measurements provided by the Langmuir Probe (LP) on board Swarm LEOs, DORIS and ground-based GNSS co-located measurements, as it is described in the paper. In this way we conclude the possible detection of the tsunami related ionospheric gravity wave in PNG 2016 event, consistent with the most-recent theory which shows that a tsunami (which is localized in space and time) excites a spectrum of gravity waves, some of which have faster horizontal phase speeds than the tsunami. We believe that this work shows as well the feasibility of a future potential monitoring system of ionospheric disturbances, to be made possible by hundreds of cubesats with POD GNSS receivers among other appropriate sensors, and supported for real-time or near real-time confirmation and characterization by thousands of worldwide existing ground GNSS receivers.**

***Index Terms*—Global Navigation Satellite System, Low Earth Orbit Satellite, Ionospheric Indicator of Earthquake/Tsunami**

Corresponding author: manuel.hernandez@upc.edu

H. Yang was with the School of Electronic Information and Engineering, Yangtze Normal University, 408100 Chongqing, China. He was with the Department of Mathematics, IonSAT, Universitat Politècnica de Catalunya, 08034 Barcelona, Spain.

M. Hernández-Pajares was with the Department of Mathematics, IonSAT, Universitat Politècnica de Catalunya, 08034 Barcelona, Spain. He was with IEEC-CTE-CRAE, Institut d'Estudis Espacials de Catalunya, 08034 Barcelona, Spain.

W. Jarmołowski, P. Wielgosz, A. Krypiak-Gregorczyk and B. Milanowska were with Faculty of Geoengineering, University of Warmia and Mazury in Olsztyn, Oczapowskiego str. 2, 10-719 Olsztyn, Poland.

S. L. Vadas was with NorthWest Research Associates, Inc.; 3380 Mitchell Lane; Boulder, CO 80301, USA

O. L. Colombo was with G.E.S.T./NASA Goddard Space Flight Center, Code 926, Greenbelt, Maryland 20771, USA.

E. Monte-Moreno was with Department of Signal Theory and Communications, TALP, Universitat Politècnica de Catalunya, 08034 Barcelona, Spain.

A. Garcia-Rigo was with IEEC-CTE-CRAE, Institut d'Estudis Espacials de Catalunya, 08034 Barcelona, Spain. He was with the Department of Mathematics, IonSAT, Universitat Politècnica de Catalunya, 08034 Barcelona, Spain.

V. Graffigna was with UNLP, La Plata, Argentina. She was with the Department of Mathematics, IonSAT, Universitat Politècnica de Catalunya, 08034 Barcelona, Spain.

P. Bofill-Soliguer was with Dept. Computers Architecture, CAP-STH, Universitat Politècnica de Catalunya, 08034 Barcelona, Spain.

G. Olivares-Pulido and Q. Liu were with the Department of Mathematics, IonSAT, Universitat Politècnica de Catalunya, 08034 Barcelona, Spain.

R. Haagmans was with European Space Agency, ESTEC, Keplerlaan 1, NL-2201 AZ, Noordwijk, The Netherlands.

I. Introduction

THE coupling of earthquakes and tsunamis with the atmosphere can occur through atmospheric acoustic-gravity waves generated by vertical and horizontal displacements of the ground or sea surface [1], [2], [3], [4], [5]. Such acoustic-gravity waves propagate upward through the lower atmosphere (up to 50 km, comprising the troposphere and stratosphere) to the upper atmosphere (heights of 50 to 600 km, including the mesosphere and thermosphere) [6]. Due to the exponential decrease of the particle density with increasing altitude and the conservation of the energy [7], the amplitudes of fast gravity waves (with initially small amplitudes such as occurs with tsunamis) will increase exponentially with altitude until they are dissipated by the exponentially-increasing kinematic viscosity in the thermosphere [5], [8], [9]. Until damped by molecular viscosity, these gravity waves induce Traveling Ionospheric Disturbances (TIDs) through neutral-ion collisions. These TIDs are not self-sustaining, though; once a gravity wave is dissipated, it no longer induces a TID.

Through neutral-ion collisions, the ionospheric delay of the carrier phase and pseudorange GNSS measurements gathered by ground and on-board Low Earth Orbit (LEO) receivers from +100 transmitters orbiting above 19000 km height, is correspondingly affected [10]. In this way the geometry-free combinations of dual-frequency GNSS carrier phase measurements allow to measure such earthquake and tsunami related ionospheric signatures very accurately, typically from the ground (e.g. [11]). The possibility of doing this procedure automatically from available LEO-based GNSS receivers intended for Precise Orbit Determination (POD), is the main challenge studied in this work.

We present two case studies using event-collocated passes of Swarm satellites. The events were the Papua New Guinea Mw7.9 and Solomon Islands Mw7.8 earthquakes both occurred in 2016. Swarm satellites carry on both POD GNSS receivers, providing Total Electron Content (TEC) measurements, and a Langmuir-probe measuring the in-situ electron density, which are useful in order to validate the detection of

anomalous TEC perturbations. The validation is completed by analyzing the ground-based GNSS data and DORIS measurements.

Dual-frequency GNSS receivers have become one of the most precise and with widest coverage ionospheric sounding technique in the present times, see for instance a reliable GNSS ionospheric monitoring in [12]. In line with the above, [11], [13], [14], [15] and [16] reported the detailed evolution of the ionospheric response to earthquakes and tsunamis, mostly in terms of TIDs, using large-scale networks of ground-based GPS receivers. This wide observational capability of GNSS contrasts with specific and local observations, such as digital Doppler sounders [17], and the OI(^{3}P-^{1}D) 630.0 nm airglow imagers [4].

The TIDs induced by atmospheric acoustic-gravity waves via neutral-ion collisions can be characterized by ionospheric measurement in the line-of-sight path from the ground-based GNSS receiver to the satellite. The medium-scale TID activities are normally assumed to occur below the maximum height of the F2 layer, where fast gravity waves can propagate and a sufficient amount of ionized particles interact with the neutral atmosphere [18]. By assuming this hypothesis the horizontal behaviour of TIDs can be well characterised by ground-based GNSS equipment, while neglecting the vertical position and altitude-related characteristics.

LEO satellites, deployed in orbits at altitudes from several hundred to more than a thousand kilometres, provide the opportunity to independently observe the topside ionospheric response to earthquakes and tsunamis by processing Precise Orbit Determination (POD) data from space-borne dual/multi-frequency GNSS receivers with a positive elevation angle. As an illustration, [19] and [20] observed the ionospheric disturbances induced by the 2011 Japan Tohoku earthquake from the GPS POD data of the GRACE LEO satellites above the U.S. Alaska region. [21] and [22] also reported the topside ionospheric response to 2015 Chile tsunami from the POD data of Swarm and GOCE LEO satellites which was confirmed by other in-situ instruments.

In addition, the footprints of earthquakes and tsunamis can also be recorded by alternative measurements taken from LEO satellites, e.g. the seismic signal measured in the middle ionosphere from the range data between two GRACE satellites [23], as well as from the co-seismic gravity gradient data of the GOCE satellite [24]. The tsunami-driven gravity waves were also measured by the ionospheric radio occultation (RO) data from COSMIC satellites [25], accelerometer and thruster in the GOCE satellite [26], the Langmuir Probes of Swarm satellites [21], and K/Ka-band interferometer of GRACE satellites [22].

In summary, the use of a large-scale, densely distributed ground-based GNSS observation network has allowed so far a remarkable reconstruction of the detailed characteristics of the near-coast ionospheric footprint of medium- and large-scale earthquakes and tsunamis. This enables a rough estimate of the location and intensity of the earthquake and tsunami [2], [27], [28], and it also makes possible to establish an early earthquake and tsunami monitoring system [11], [29].

With the addition of LEO satellites that could observe tsunami ionospheric features far from land, the use of multi-source observations would contribute to increase the effectiveness of the monitoring system [30]. However, it should be noted that there are a priori challenges in definitively capturing topside TID activities of earthquakes and tsunamis by on-board POD GNSS observations and other instruments: a) the LEO satellites should properly cover in space and time the target regions, which will be facilitated by the ongoing plans of deploying hundreds of LEOs with on-board GNSS POD receivers; and b) the intensity of the released energy should allow to induce topside ionospheric activity with a detectable intensity. In this regard, and by employing all available observations from the Swarm LEO satellites during years, [31] reported a possible connection to earthquakes through in-situ detected anomalies in electron density (ED) and magnetic field data.

With the above context in consideration, in this paper we show the potential capability for POD-GNSS receiver measurements from LEO satellites, orbiting at 450 km and above, to detect anomalous ionospheric disturbances (including those associated with earthquakes and tsunamis). This claim is based on two facts:

1) A single Chapman model with a linearly increasing height scale describes very well the behaviour of the ED above the LEO height (typically above the peak of the F2 layer), ([32], [33], which, for instance, allows accurate extrapolation ([34], [35]). The smooth behaviour at the topside ED allows the measurement of clear signals of an earthquake or tsunami despite the relatively low ionisation level and the high elevation at the location of the event.
2) The increasing number of cubesat constellations which might allow in the future a 24/7 applicability of the technique proposed in this work. Currently, there are several hundred cubesats that can perform ionospheric sounding with GNSS signals. Some companies have deployed cubesats for RO ionospheric sounding successfully [36], [37], despite initial problems due to size and power (e.g. duty cycling impact, see for instance [38]).

We propose in this work a methodology that potentially detects earthquake and tsunami related signatures in the topside ionosphere, mainly based on the POD data from GNSS receivers on board LEO satellites: This method is called the PIES approach (*POD-GNSS LEO Detrended Ionospheric Electron Content Significant Deviations* technique). PIES extends the applicability and scope of our previous multi-technique study of Chile-Illapel 2015 Mw8.3 event [39] to other events. The method includes three steps: the acquisition of significant characteristics, the identification and issuance of warnings, and the external validation. This technique might be able to provide potential warnings of earthquakes and tsunamis relying only on GNSS POD observations from future dense constellations of LEO satellites.

We illustrate the application of the PIES methodology to the detection of the possible topside-ionosphere footprints from two earthquakes/tsunamis by using the data of LEO satellites that passed near the respective epicenters at the time of the events:

- On 17 December 2016 a Mw7.9 earthquake and tsunami

happened at Papua New Guinea (PNG). We will show how PIES discloses potential earthquake and tsunami ionospheric signatures thanks to the availability of nearby Swarm POD GNSS data. This anomaly is further confirmed by in-situ Swarm Langmuir Probe (LP) ED and ground based GNSS data.

- In the Solomon Islands 2016 event, a Mw7.8 earthquake and tsunami happened on 8 December 2016, and after applying PIES in a blind way, an important pre-seismic disturbance was detected. Such ionospheric perturbation has been validated by multiple ionospheric measurements such as Swarm LP, ground GNSS and DORIS data. The origin of this perturbation was checked out, but no conventional sources could be found to explain it, including meteorological events. This case study is considered of interest by itself to show the capabilities of PIES as a blind LEO-based anomalous ionospheric perturbation detector.

II. Description of Experimental Data

A. Measurements

In this study, the POD data of dual-frequency GPS observations from Swarm LEO satellites is used to test the proposed method for detecting the upper anomalous ionospheric perturbations potentially including those originated from earthquakes and tsunamis. The Swarm LEO constellation, composed of three identical quasi-polar orbiting satellites of European Space Agency (ESA), began to provide 1 Hz GPS observations in middle 2014 [40]. Two of them (Swarm A and C) placed at the orbit of $\sim$460 km altitude, and the other (Swarm B) at $\sim$510 km, can record the topside ionospheric activity by GPS POD receivers. The fly design of Swarm A and C, in parallel with a horizontal distance of less than 200 km, facilitates detailed observation of the wavefront motion that can contribute to the analysis of the response of the top ionosphere to atmospheric gravity waves driven by seismic tsunamis.

In addition, other measurements are employed for the validation of the detected data from POD: a) LP measurement on Swarm satellites for in-situ ED; b) GNSS POD measurement from other LEO satellites; c) GNSS dual-frequency observation of ground network for high-resolution slant total electron content (STEC) along the line of sight between GNSS satellites and receivers; d) DORIS dual-frequency measurement for bottom ionospheric activity (see an example of application in [41]); e) wind field observation for the background neutral wind activity; f) meteorological data and earthquake/tsunami records for confirmation of the potential origin of the ionospheric deviation.

B. Selection of Earthquake/Tsunami Cases

We have found two neighbour regions, PNG and Solomon islands, where two earthquakes occured colocated with the passes of Swarm satellites during the studied period, end of 2016. In particular, PNG is located at the connection of four main tectonic plates: Australian, Pacific, Eurasian and Philippine plates. There are also a number of smaller plates, which makes this region especially active seismically. The time period selected for the analysis covers November and December of 2016. November is relatively seismologically quiet, and includes two weeks, during which no earthquake of magnitude equal to or above 5.0 occurred. The threshold 5.0 for the selection of earthquakes in this work is assumed approximately, by inferring from the existing works on the sensitivity of ground GNSS data to the seismic activity (see [42], [43]), as well as from recent works on the sensitivity of Swarm magnetic data to earthquakes of similar magnitude [44]. December 2016 was very active seismologically with two earthquake events having magnitude 7.8 and 7.9, both triggering tsunamis. There were almost 150 earthquakes equal or above the magnitude 5.0 from the beginning of November 2016 to the end of the December 2016, the most of which were aftershocks and took place after 8 December 2016. The orbits of Swarm satellites, which have inclination around 87.35°, pass the edge of two subducting tectonic plates (Australian and Pacific) at a quite large angle.

III. Techniques for Detection and Validation

In this section, the techniques for detecting and recognizing significant topside ionospheric disturbances in the spectral range of the earthquake and tsunami ionospheric footprints from GNSS POD data will be described in detail. The approaches used for validation have been the evolutionary power spectrum technique for analysing ED from LP measurement, as well as the simple detrending technique for analysing other measurements such as DORIS and ground GNSS observations.

A. PIES: POD-GNSS LEO Detrended Ionospheric Electron Content Significant Deviations

One challenge in the sounding of the ionosphere by GNSS POD data, and by any other on-board instrument, such as the LP measuring in-situ electron density, is that the LEO satellites move at high-speed (e.g. around 7.5 km/s for the Swarm satellites). This fact makes it difficult to determine the local response of the ionosphere to a given event, which requires the LEO satellite to pass close to the region at the time of the event, i.e., at a distance of less than several hundreds km from the epicentre. This is the typical distance between the representative points of the ionospheric measurements of different GNSS transmitters observed from a given LEO POD GNSS receiver[1], which allows some of them to be located very close to the epicentre. Fortunately, the availability of more LEO satellites can definitely provide enhanced ionospheric sounding.

For each given region of interest, PIES requires the time series of detrended ionospheric electron content from GNSS POD data, finds out the significant disturbances by excluding the signatures of known origins and comparing with adjacent (previous, in real-time functioning) normal days, and finally validates the disturbance detection from other measurements. The PIES approach comprises two principal phases summarized in the next two subsections, and each of them includes different steps (see Figure 1).

[1]known as *Ionospheric Pierce Points* (IPPs) in the GNSS community

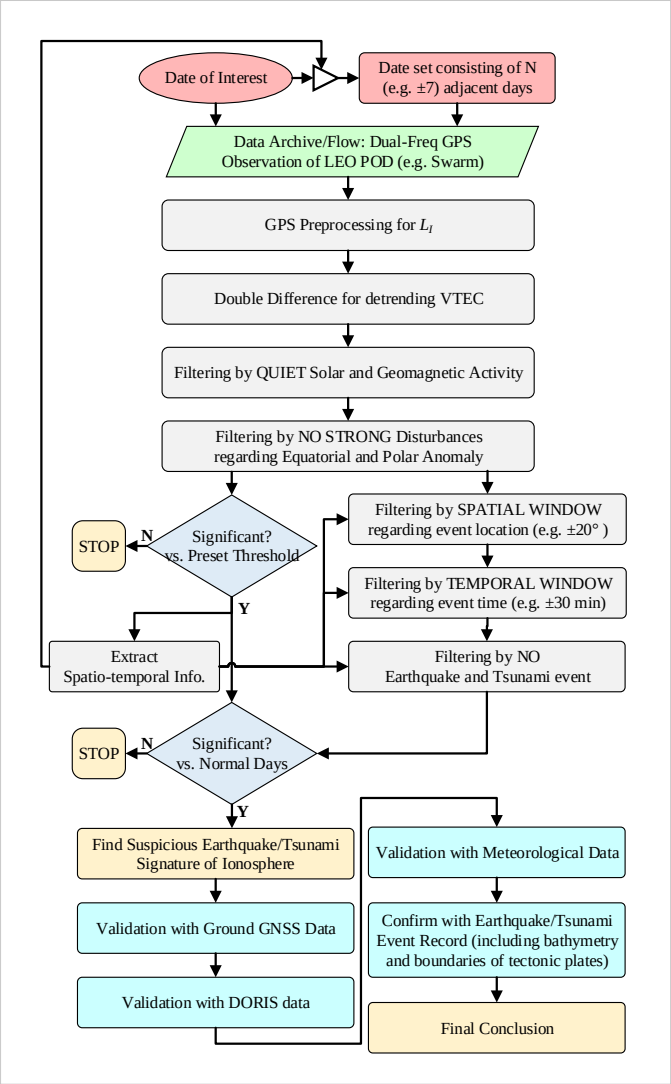

Fig. 1. Flow chart of PIES.

1) PIES first step: Ionospheric Wave Signature retrieval from GNSS POD data: The orbital speed of the LEOs, v_{LEO}, (7.5 km/s for the Swarm satellites), is way higher than the highest horizontal velocities v_{TID} of the possible ionospheric signals to be detected by the LEO (e.g. from few hundreds of m/s for gravity waves [13] to 1 km/s around 450 km height for the acoustic waves following Figure 1 in [45]). Therefore, the sounding from the LEO is considered as a snapshot of any crossing ionospheric wave. In this way, we can easily estimate the ionospheric wave $\lambda_{TID} \simeq v_{LEO} \cdot T_{TID@LEO}$ from the observed periods $T_{TID@LEO}$ with the highest energy. Then we can calculate the approximate actual period $T_{TID} \simeq \lambda_{TID}/v_{TID}$ from the estimated TID horizontal velocity v_{TID} (see points 3 and 4 at next -second- PIES step), taking into account as well the relative movement LEO - ionospheric wave. This is important in order to determine whether the actual wave period is above or below the buoyancy period, around 5-8 minutes [46], i.e. to figure out whether we are detecting a gravity or an acoustic wave. Another aspect to double check what kind of wave we are sensing is to estimate the vertical velocity which should be at least 300 m/s for an acoustic wave, being likely a gravity wave for lower values.

The main observation in PIES is the ionospheric combination (also called geometry-free combination) $L_I = L_1 - L_2$ of the carrier phase measurements L_1 and L_2 in both GPS POD receiver frequencies and expressed in length units. As it is well known, L_I mainly depends linearly on the along line-of-sight integrated ionospheric electron density, i.e. STEC or (S), and on the carrier phase ambiguity $B_I = B_1 - B_2$, which can be considered constant for each phase-continuous transmitter-receiver arc, and then completely removed after a simple detrending (see the review paper [10] for details after a general introduction on *GNSS Ionosphere*).

S mainly contains typical trends of total electron content such as diurnal variations and elevation angle variation, which are characterized by extremely low frequencies and very high energies. It also contains ionospheric perturbations with lower energies at higher frequencies, like Medium Scale Travelling Ionospheric Disturbances (MSTIDs, see for example [47]), including the circular wave signature of earthquakes and tsunamis [11].

Instead of the typical usage of bandpass filters to separate the disturbance components, PIES uses an alternative efficient solution directly based on the double time difference of the measured ionospheric combination of carrier phases, L_I. The detrended STEC can be directly obtained as $\tilde{S} \approx L_I(t) - \frac{1}{2}\left(L_I(t-\tau) + L_I(t+\tau)\right) = \frac{-1}{2}\delta^2 L_I$. In this way, the phase bias of L_I, constant in continuous phase arcs (i.e. in between cycle-slips), cancels out. Furthermore, the energy of trend components decreases, and, at the same time, the terms with periods T around twice the time interval τ considered in the double time difference, are amplified (see details in [18]).

Moreover, the motion of the ionospheric observing points is taken into account in PIES. It is especially significant in our scenario of LEO-based measurements where the GNSS receivers are moving at very high speed, up to more than one order of magnitude higher than the ionospheric waves. The corresponding effect in the expected periods[2] can be considered in a simple way in PIES: assuming, as it has been commented above, that the ionospheric waves appear almost "frozen" in front of the fast movement of the sensors (like the GNSS POD receiver and LP) on-board the LEO. Considering as well different orientations between the LEO and the ionospheric wave velocities, the range of potential periods of earthquake- and tsunami-related ionospheric TIDs measured from Swarm LEOs goes approximately from 10 sec to 240 sec.

The selection of the optimal time difference $\widehat{\tau}$ to perform the double-time difference detrending allows to reveal the ionospheric response to the tsunami.

In PIES, the mapping function M approximation is applied. In other words, it is considered that the modelled detrended Vertical Total Electron Content (VTEC, defined as $\tilde{V}$), which can be derived from the LEO STEC ($\tilde{S} = \tilde{V} \cdot M$), see [10], is located on a spherical thin-shell layer placed at a mean effective height. Such approximation works better at

[2]the Doppler effect

high than low elevation angle. Therefore, in order to reduce the ionospheric mismodelling the mapping function hypothesis may yield, the observations with an elevation angle of less than 40° are discarded.

2) PIES second step: Warning of potential anomalous ionospheric signature: A warning of potential anomalous ionospheric disturbance will be issued by PIES once a sudden increase appears in the temporal evolution of the power of the detrended VTEC $\tilde{V}$ on the passes of the LEO satellite. Such increase is estimated by comparison with the previous $\tilde{V}$ values measured in the same region and at similar times. In this way, the seasonal ionospheric signatures like those of seasonal MSTIDs, are not taken into account implicitly. In order for the PIES to declare an ionospheric disturbance as potentially significant, the following evidence must be met:

1) **Comparison with a record of adjacent normal days**: Note that some of disturbances of different origin are difficult to distinguish from the tsunami-driven ones. This is due to them having quite similar features in terms of time and frequency (see for instance MSTID climatology in [47], [11]). The adopted solution in PIES is to compare the disturbances with the record of previous $2 \cdot n$ days in real-time or $\pm n$ days in post-processing (e.g. with $n = 8$ or $n = 13$), by means of an identical spatial window (e.g. $\pm$20 degree w.r.t the location of the event), time of day window ($\pm$30-90 min w.r.t the time of the event), and the normal day window that filters out the days with strong activity due to either space weather or any earthquake/tsunami events.
2) **Discard disturbances regarding space weather or equatorial/polar anomalies**: It is possible that the detected ionospheric waves are induced by unusual conditions of space weather, like the strong solar activity or geomagnetic activity. Alternatively, there could be ionospheric anomalies as the LEO satellites pass over equatorial and polar regions. Therefore, those components of the disturbances, corresponding to expected equatorial and polar regions ionospheric anomalies, will be dropped.
3) **Estimation of propagation parameters in time and space**: The determination for the propagation parameters should be done ideally in real-time when possible, or at least in near real-time, by means of rapid and efficient determination models or algorithms, such as, for example:
   - the rough parameter inspection from time and frequency analysis for the POD GNSS observation of a single LEO satellite compared with velocity estimations from keograms based on MSTID-detrended L_I from ground based GNSS receivers;
   - or the technique of direct GNSS Ionospheric Interferometry (see [48]) for the case when tandem LEO satellites (such as in Swarm case) are available.
   - or, alternatively, the Atomic Decomposition Detector of MSTIDs technique provides as well velocity estimation, when a minimum density and number of permanent ground based GNSS receivers is available [49], [11].
4) **Confirm spatio-temporal propagation consistency with earthquake/tsunami source**: The estimated propagation parameters allow for the exclusion of components of ionospheric signature that have low relevance compared with the earthquake and/or tsunami contribution. Thus, the ionospheric signature would be excluded or marked as "low confidence". The spatio-temporal information related to the disturbances that are compatible with the propagation of the tsunami is retrieved and compared with additional information for double checking the feasibility of the earthquake/tsunami signature detection. An example is the consistency of the velocity evolution of the detected TID signal compared with the sea floor depth changes. The above considerations are used, for instance, to declare or not the PIES warning of a potential tsunami.

B. Short Term Fourier Transform and Time Varying Electron Density Power Spectra

The discrete Fourier transform (DFT) decomposes discrete signals in sinusoidal components which model the features that are useful for the additional validation of the potential earthquake or tsunami ionospheric footprint detection, beyond the simple PIES detrending procedure previously introduced. The signal of time samples function $x(t)$ can be decomposed into frequency components $X(\omega)$ covering the entire ω discrete frequency range. This frequency domain representation can be also transformed back exactly to $x(t)$ by the inverse Discrete Fourier transform. The square of the absolute value of the DFT values in the frequency domain provide the spectral power density at individual frequencies.

An efficient method of signal analysis in time is short-time Fourier transform ($STFT$), which is time-wise, sliding window of DFT applied sequentially on the input signal. This sliding window procedure allows for tracking the change of position of the spectral peaks. The STFT plots allow to characterize the sequential time changes of the signal in the frequency domain. The evolutionary and windowed power spectrum is a modification of the DFT method, which computes the spectrum of overlapping segments of the time series. The evolutionary power spectrum can be calculated by the STFT. The output of $STFT$ is the short-term, time-localized frequency power of the signal. The data sequence to be transformed is multiplied by a window function which is nonzero for only a short period of time [50]. The $STFT$ of the signal is computed as the window is sliding along the time axis, resulting in a two-dimensional representation of the signal. Mathematically, this is expressed as:

$$STFT_{f,t} = \sum_{n=0}^{N-1} x_n w_{n-t} W_N^{fn}, f = 1, 2, ..., N-1 \qquad (1)$$

where x_n is a sequence of discretized time-domain signal to be transformed, f is harmonic number, n is the number of sample, N is the number of all samples, $W_N = e^{\frac{i2\pi}{N}}$ and w_n is a sequence of a discretized window function and t is its time sample index. The applied window is Tukey window. Tukey window, also known as the cosine-tapered window, can be regarded as a cosine lobe of width $\frac{r}{2}(N-1)$ that is convolved with a rectangular window of width $(1 - \frac{r}{2})(N-1)$. The

function of the window is to reduce the variability associated with the Periodogram. The equations defining Tukey window $w_{TU}(n)$ are:

$$\begin{cases} \frac{1}{2}\left[1+\cos\left(\frac{2\pi}{r}\frac{n-1}{N-1}-\pi\right)\right], & n < \frac{r}{2}(N-1)+1 \\ \frac{1}{2}\left[1+\cos\left(\frac{2\pi}{r}-\frac{2\pi}{r}\frac{n-1}{N-1}-\pi\right)\right], & N-\frac{r}{2}(N-1) < n \\ 1, & \text{otherwise.} \end{cases} \tag{2}$$

where r is the ratio of taper to constant sections and is between 0 and 1.

For fixed time, $STFT$ of a data sequence x_n describes its local frequency content near the sample at moment t as a function of the discrete frequency f. These frequency representations form then the image or a three-dimensional surface, the shape of which depends on the window size and overlap size. This essentially corresponds to computation of the STFT squared magnitude of the signal sequence x_n — that is, for a window width n, as follows:

$$SP_{f,t} = |STFT_{f,t}|^2 \tag{3}$$

C. Other Validation Approaches for PIES Warning

Once a potential warning of earthquake-/tsunami-driven disturbances by PIES is issued, the warning validation should be done in the next stage. This validation can be based on different ionospheric observation approaches:

a) Validation with ground GNSS Data and other LEO GNSS Data: The ground GNSS data, in PIES approach, provide a reliable way of confirming the potential tsunami/earthquake related ionospheric warnings provided by Swarm, based on its heritage in the TID modeling (see for instance [47], [48]) and the recent improvements, especially with dense and large networks with a positive impact in its application for studying composed phenomena [49], [51], [11].
b) Validation with DORIS Data: DORIS dual-frequency measurements, at 2036.25 MHz (S1) and 401.25 MHz (U2), from the 51 ground transmitters to the 5 available LEO POD onboard, like Cryosat-2 (CS2), JASON-3 (JA3), HY-2A (H2A), Sentinel-3 (S3A) and Saral (SRL) flying at different LEO heights, have been also considered in this study. They contribute to the validation of the results under PIES obtained associated to PNG and Solomon Islands earthquakes and tsunamis, providing a detrended TEC measurements below the DORIS transmitters on board such a LEOs.
c) Validation with the multi-GNSS and multi-system ionospheric tomography, including DORIS data as well [41].
d) Validation with Meteorological Data: The background wind data on neutral atmosphere will be investigated as well. This can allow discarding a strong wind event in the lower to middle atmosphere that might influence the AGW propagation [52], and create potential tertiary gravity waves that originate from the dissipation of mountain waves [53], [54]. Strong rainfall events can be checked as well, following recent results in [55]), looking for instance in [56].

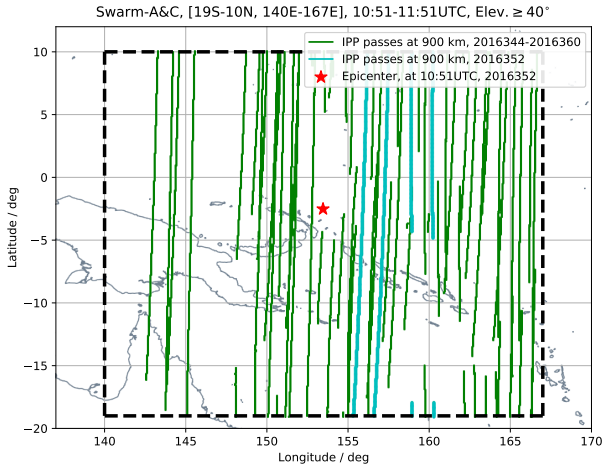

Fig. 2. Location of the ionospheric observations (in cyan) of Swarm A&C regarding GPS satellites within 1 hour after the main shock of 2016 PNG earthquake, at few hundreds kilometres east from epicentre, with a spatial window (140°E–167°E vs. 19°S–10°N), with an elevation mask of 40°. The green lines correspond to the 16 adjacent normal days, with the same spatio-temporal window, and elevation mask as the earthquake day, and the red star for the epicentre.

e) Confirmation with Earthquake/Tsunami Event Record: Investigate the occurring location and time of disturbance if it shows the coherent characteristics with tsunami, e.g., the velocity of disturbances similar to the tsunami along bathymetry and boundaries of tectonic plates.
f) Comparison with hydrodynamic models of the ocean to predict the size, shape and likely path of tsunami disturbances to help confirm or correct the hydro model results using the satellite ionospheric footprint derived results [57], and vice versa.

The final PIES warning is released once the disturbances are confirmed by other approaches of ionospheric sounding.

IV. 2016 Papua New Guinea Event: Anomalous Ionosphere Signature from Swarm POD

On 17 December 2016, a tsunami event occurred in PNG, giving rise to a maximum height of 1 meter, which was triggered by a 7.9 magnitude earthquake that occurred at 10:51:12 UTC.

We selected this first event because the Swarm satellites A and C passed few hundreds kilometres east of the epicentre, about 45 minutes after the main earthquake shock. The trajectories of the representative points of the ionospheric GNSS POD receiver observations (in cyan points) vs. the epicentre (in red star) are shown in Figure 2. We took a proxy value of 900 km height for computing them, which is suitable under the adopted elevation mask of 40° deg and the associated small ionospheric mapping function error affecting the VTEC estimation. Then we had the chance to see if the corresponding POD GPS observations might contain an anomalous ionospheric footprint.

A. Inspection of PIES Warning

As a first step to apply the PIES technique introduced in section III-A, the ionospheric signatures with time steps of $\{\tau = 2^k : k = 0 \dots 8\}$ sec $= \{1, 2, 4, 8, 16, 32, 64, 128, 264\}$ sec are searched from the corresponding double time difference detrending of the three Swarm GPS POD receivers (Swarm-A, B and C), and they are compared with the values at the same region up to one week before and after (in real-time mode up to few weeks before). Taken into account the expected range of ionospheric wave periods discussed in subsection III-A1, the initialization of the double difference (i.e. the band pass filter) would be done by looking for the optimal time step. The resulting detrended values (Figure 3) clearly show one period, associated in particular to a time difference of $\tau = 8$ sec (i.e. a maximum relative energy at a period of $T = 16$ sec), where the energy is the larger one during the whole period analysed of 17 days of Swarm passes. This is compatible with the expected apparent periods previously discussed, and was confirmed by examining the maximum ratio of the energy of the disturbances within 1 h during the main shock with respect to the energy within the same spatial window during 16 adjacent days, see again Figure 3. Note that the other distinct disturbances in Figure 3D, such as those on days 344, 353, 354, and 356 in 2016, contain significant low-frequency components, as confirmed by the double-differential bandpass filtering results with different time intervals, see the results in Figures 3G, 3H, and 3I. Compared to the PNG earthquake/tsunami of interest, these disturbances exhibiting different types of characteristics may be driven by different sources which are seen as data noise in this work.

Note that a spatial window of 140°E–167°E vs. 19°S–10°N is employed for looking for significant detrended VTEC values. The target time interval is about 10:00–12:00 UTC (i.e. 20:20–22:20 in local night), when the equatorial effect of the ionosphere would not be significant. The geomagnetic equatorial index *Dst* = 3 nT [58], the planetary 3-hour-range index *Kp* = 3 [59], and the GOES X-ray flux measurement of Class-A [60] all indicate quiet space weather conditions, with no significant disturbances originated by these phenomena such as major solar activity, solar flare, or geomagnetic storm disturbances.

The detrended VTEC was computed by the double time difference with the optimal time step of 8 sec. This showed the significant disturbances about 45 min after the earthquake/tsunami. The possible confounders were also tested and their presence was ruled out. The disturbances located several hundreds kilometres from the epicentre exhibit a signature compatible with the response to the tsunami both horizontally in time and space. Since tsunami-driven disturbances display propagation parameters similar to those of MSTIDs, in PIES application we have used the ionospheric state on 16 adjacent normal days, as a reference for discarding that the disturbances detected are seasonal features of ionospheric disturbances. Note that for this event these normal days are not affected by strong space weather records, see the location of the ionospheric observations in green in Figure 2. Figure 4 shows that the zoomed view of the results presents the most significant detrended VTEC during 1 hour after the main shock.

The much stronger power of the disturbances on the earthquake day compared to that on the normal days might indicate the ionospheric response to the earthquake/tsunami. Two GPS receivers onboard Swarm A & C provided the observations right after the main shock (Mw 7.9), sensing at elevation angle above LEO horizon ($\geq$40°). Regarding GPS satellite PRN 32, the line-of-sights that crossed the full main shock target region from the north to south, show the maximum power of the disturbances. Figure 5a shows the detrended VTEC regarding GPS satellite PRN 32 and Swarm A & C. Most pronounced VTEC oscillations reach Swarm A before Swarm C, i.e. in order of 3D distance to epicentre (see Figure 5b).

Considering the tsunami wave distribution in space and time, this signal might have an associated frequency compatible with the expected one for tsunamis and detected around 45 minutes after the earthquake. It might also be related with the tsunami due to its appearance at this time and distance from epicentre, but also in this region located in the south to the chain of islands. The furthermost distant satellite (Swarm C) appears as the most affected, especially at the south of chain of islands: it might be that Swarm C reached "on time" the region where the tsunami induced some ionospheric disturbance signals, whereas Swarm A would have been "late", except for the biggest signal which would correspond to different waves (otherwise the travel time between them would be too short, ∼20 sec for ∼100 km). In any case, the signals, not aligned regarding to the epicentre, might correspond to different wavefronts, which would be consistent with the circular ionospheric acoustic-gravity waves reported in [11].

Once the main target of the new PIES technique is fulfilled (i.e. detection and warning on anomalous ionospheric wave signatures), we proceed to estimate the type of ionospheric wave. This is done by estimating the ionospheric wavelength first, and then the actual period. Additionally, the vertical velocity is also estimated for such goal.

Following the above introduced notation, the horizontal wavelength of the TID, λ, can be estimated as $\lambda \simeq v_{LEO} \cdot cos\beta \cdot T_{TID@LEO} \simeq$ 130-260 km. Assuming that the wavefront propagates with spherical symmetry, β is the angle between the LEO velocity and the wavefront propagation directions. For the location of the highest detected detrended peak in Figure 5B, $\beta \simeq 30°$. The dominant period components $T_{TID@LEO} \simeq$ 20-40 sec can be directly observed from spectrograms of the detrended VTEC of Swarm A and C (see Figure 11 and 13) at ∼11:35 UTC, when the disturbances are of highest intensity. Note a different but much weaker component $T_{TID@LEO} \simeq$ 30-40 sec is shown between 11:32–11:34 UTC, particularly indicated in Figure 13. As an independent measurements for TIDs by means of Swarm space-borne LP, the spectrograms of ED disturbances shown in Figure 10 and 12 confirm the spatial evolution of the period components. A rough estimation of the actual TID period at ∼11:35 UTC yields $T_{TID} \simeq \frac{\lambda}{v_{TID}} \simeq$ 217-433 sec, where the horizontal TID velocity $v_{TID} \simeq 600$ m/s is estimated correspondingly from the keogram Figure 7B, taking into account the horizontal distance of the epicenter-LEO pass with the disturbed signal

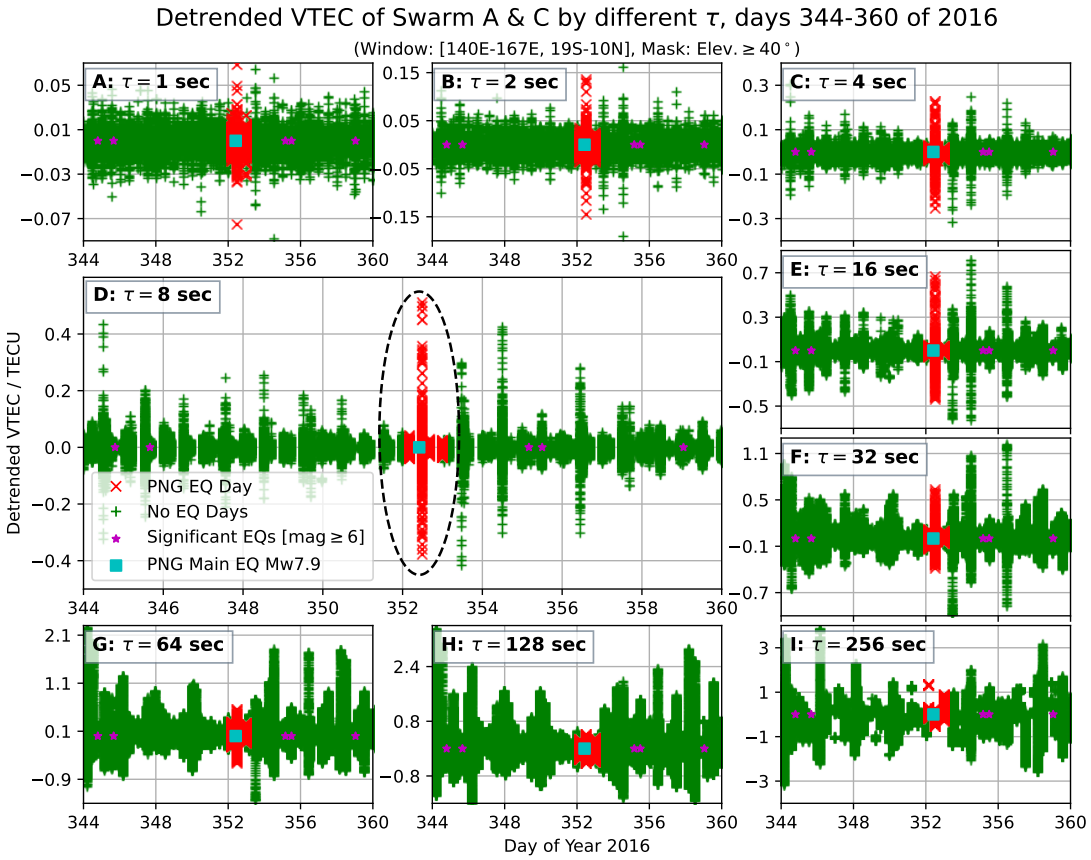

Fig. 3. The PIES detrended VTEC computed from Swarm A and C POD GPS data with an elevation mask of 40 deg is represented vs time during 17 days (in green) around the PNG earthquake, happened on 10h51m of day 352 of 2016 (with values marked in red), and for a spatial window (140°E–167°E vs. 19°S–10°N) around the epicentre. This is represented for different detrending time steps τ = 1, 2, 4, 8, 16, 32, 64, 128, and 256 sec in subplots A to I. The common legends can be seen in plot D, in large size to emphasize that the larger detrended VTEC value happens very close to the earthquake main shock, and for $\tau = 8$ sec consistently with the expected values considering the high movement of the LEO and the expected wavelengths of the ionospheric waves. The blue star for location of the significant earthquakes ($\geq$Mw 6).

and the elapsed time from the main shock to the corresponding detection time. And the approximation for the TID period during 11:32–11:34 UTC is $T_{TID} \simeq \frac{\lambda}{v_{TID}} \simeq$ 500-650 sec, with the corresponding horizontal TID velocity $v_{TID} \simeq 400$ m/s. Since the period variation of TIDs along Swarm IPP passes is associated to the horizontal distance from the epicenter, it may indicate that the proposed ionospheric disturbances have at least one more origin, such as the EQ-driven acoustic waves and the tsunami-driven gravity waves.

This estimation of $v_{TID} \simeq 400$ m/s at 11:32–11:34 UTC is a bit larger than the horizontal velocity component of the main gravity wave excited by the tsunami as it is the case (see Figure 1 at [13] and associated comments). However, these references assumed that a monochromatic gravity wave is continuously excited by a tsunami as it moves across the ocean, and that this gravity wave has the same horizontal phase speed as the tsunami. In fact, the simulated tsunami maximum amplitude, travel times and the ocean depth shown in Figure 6 indicate that the tsunami is localized in space and time, therefore an entire spectrum of gravity waves are excited [5]. This includes gravity waves traveling with the similar horizontal phase speed as the tsunami, as well as gravity waves which have much faster horizontal phase speeds [5]. These latter gravity waves reach the thermosphere faster and are less prone to dissipation from molecular viscosity, therefore they are quite important in the F region. Note that [4] observed gravity waves which had much faster horizontal phase speeds than the tsunami, thereby supporting this work.

Moreover, the guess of observed period $T_{TID} \simeq$ 217-433 sec at $\sim$11:35 UTC is similar to the above mentioned value of the buoyancy period (around 5-8 min), which indicates the option of an acoustic wave associated to the earthquake main shock. Moreover, the much greater period $T_{TID} \simeq$ 500-650 sec during 11:32–11:34 UTC show the potential detection of the gravity wave originated at the tsunami event.

In order to double check the possible tsunami origin of the measured perturbation we consider now the vertical velocity, which should be not larger than 50 m/s for a normal monochromatic wave assumption [13]. For a more realistic model, however, the vertical phase speed can be up to 300 m/s (Figure 10f and 16f of [5]). The mean vertical velocity found is also compatible with the hypothesis of the tsunami

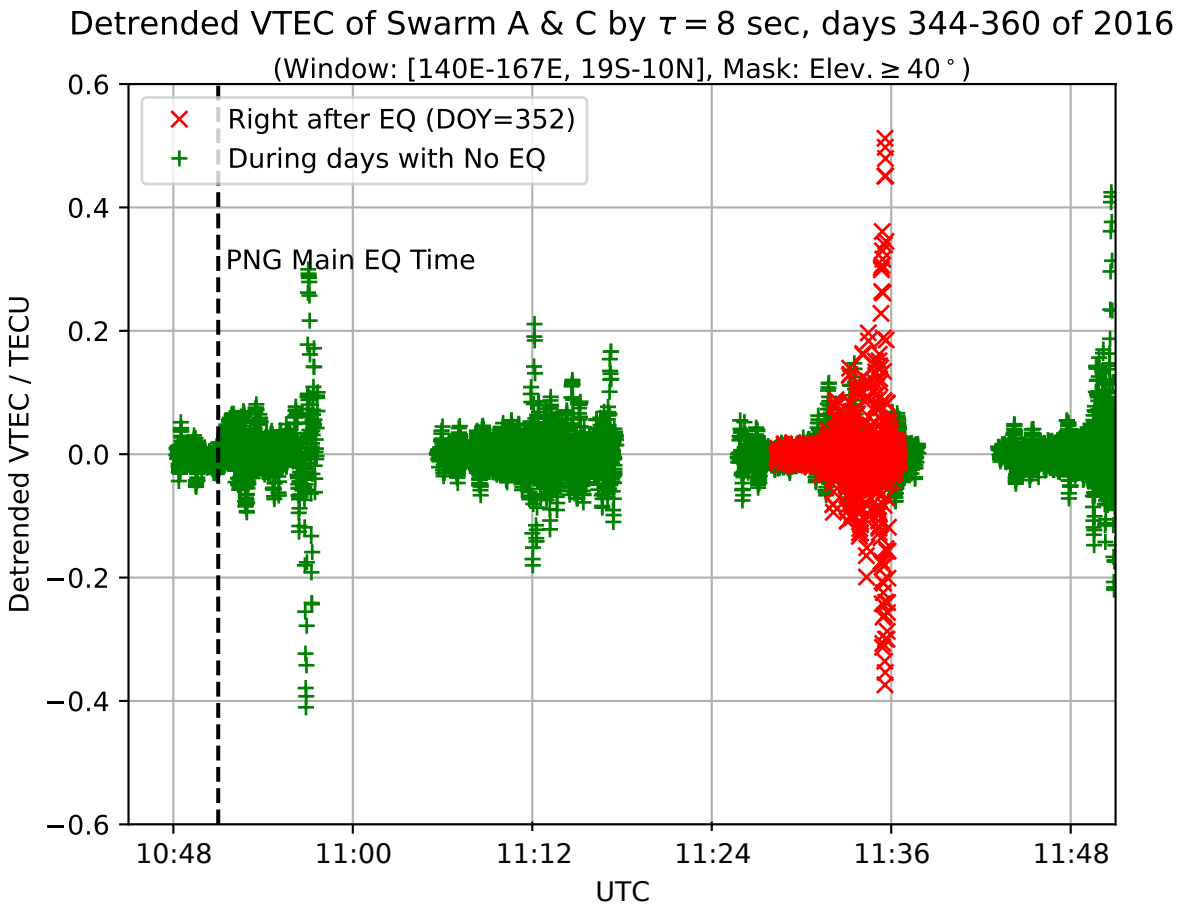

Fig. 4. Time evolution of detrended VTEC for the Swarm A and C POD GPS data already shown in previous figure (PNG earthquake, 10:51UTC of day 352, 2016) but during 1 hour after the main shock (in red scatters), compared with 16 normal days with no earthquake record (in green scatters), with τ = 8 sec. The settings of spatial window and the elevation mask see Figure 3.

origin: indeed, to reach the Swarm orbital height of 460 km with the delay shown by the largest signal after the main shock (around 45 min = 2700 sec), a vertical velocity of 460 km / 2700 sec = 170 m/s would be needed, which agrees with the model of [5], similar to [4], and significantly smaller than the vertical velocity of the acoustic waves, greater than 300 m/s.

B. Validation of Swarm A & C Langmuir Probe ED and topside TEC data by Power Spectra Analysis

In this section, the STFT analysis of ED directly measured by Swarm A and Swarm C Langmuir Probes (product from Electric Field Instrument, EFIxLP), and corresponding topside STEC from Swarm A and Swarm C (product TEC_TMS_2F), are used for confirming independently the PIES tsunami warning signal due to the detected ionospheric disturbances. This validation is supported by spectrograms of evolutionary power spectrum density (PSD), and its second purpose is to compare disturbed in-situ ED signal and topside TEC signal disturbed from the same seismic events. It should be pointed out that these two kinds of signals refer to geometrically different spatial locations and therefore an approximate similarity could be expected, rather than absolute coherency of the signals.

The analysis of Swarm A and C in situ ED and topside TEC to selected GPS satellites are based on high-pass filtered data. The Discrete Fourier Transform (DFT) has been applied for this purpose and the cut-off period was heuristically set up to 50 sec, which stems from the considerations about the sizes of seismically-driven ionospheric disturbances in the previous sections. All the data were high-pass filtered by removal of the signals with periods longer than 50 sec, then the spectral analysis by STFT was applied. The spectrograms were then sampled at 40 sec period for plotting together with GIMs in left subfigures adjoined to all spectrograms in this work. These PSD samples show their magnitudes and locations of Swarm disturbances occurring on the analysed times. The spectrograms were calculated with the use of STFT and windowing using Tukey window with its main parameter r=0.4 (see Eq. 2). The width of the window was set to 220 sec, whereas the frequency range of spectra is from 90 sec to 10 sec. The scales of the spectrograms and their samples at selected period are the same for all figures referring to the same quantity, i.e. ED or TEC.

The subject of validation are Swarm A and Swarm C corresponding trajectories, i.e. close in time and space and recorded on 17.12.2016 around 11:30 UTC, which is ∼40 min after the largest EQ (Mw=7.9) occurred close to the eastern coast of New Ireland island (10:51 UTC). Figure 8 and Figure 9 describe additional trajectories for the previous

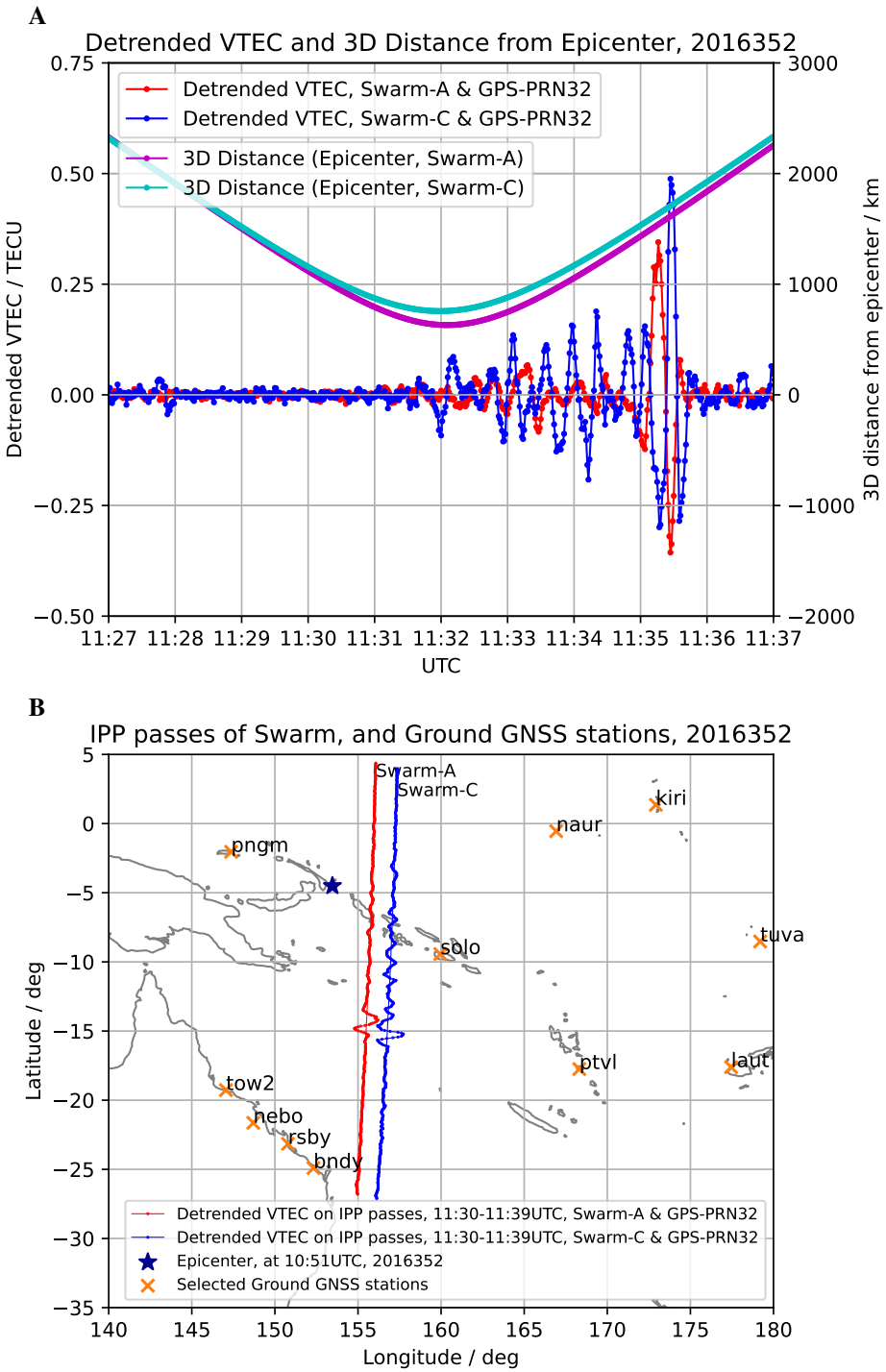

Fig. 5. A: Evolution vs time (x-axis) of 3D distance of GPS PRN 32 satellite ionospheric observation points to the epicentre of PNG earthquake (10h51m of day 352, 2016) in thousands of km (magenta and light blue lines) and the detrended VTEC in TECU (Total Electron Content Units, 1 $TECU = 10^{16} m^{-2}$), red and green lines, about 1 hour after the main shock for Swarm A & C respectively, with the settings of spatial window and elevation mask of Figure 3; B: The spatial evolution of detrended VTEC horizontally overlapping the trajectories of the observing points regarding the GPS satellite PRN 32 and Swarm A (red) & C (blue), with the epicentre marked in blue star. Nearby selected ground GNSS receivers are also represented on the map.

to EQ day, at similar time of the day. This reveals significantly smaller disturbances in ED with respect to December 17. It is easily noticeable that even if Figure 9 shows a bit larger disturbance for Swarm C ED than Figure 8 for Swarm A ED, Figure 10 and Figure 12 illustrate significantly larger perturbations after the mainshock, which confirms the meaning of major EQ having Mw=7.9.

Figure 10 shows ED spectrogram for Swarm A on December 17 at around 11:30 UTC, which is ∼40 min after Mw=7.9 EQ. Figure 11 corresponds to Figure 10 although it shows the topside TEC from dual-frequency GNSS receiver, for the selected satellite. It should be pointed out that GPS satellite

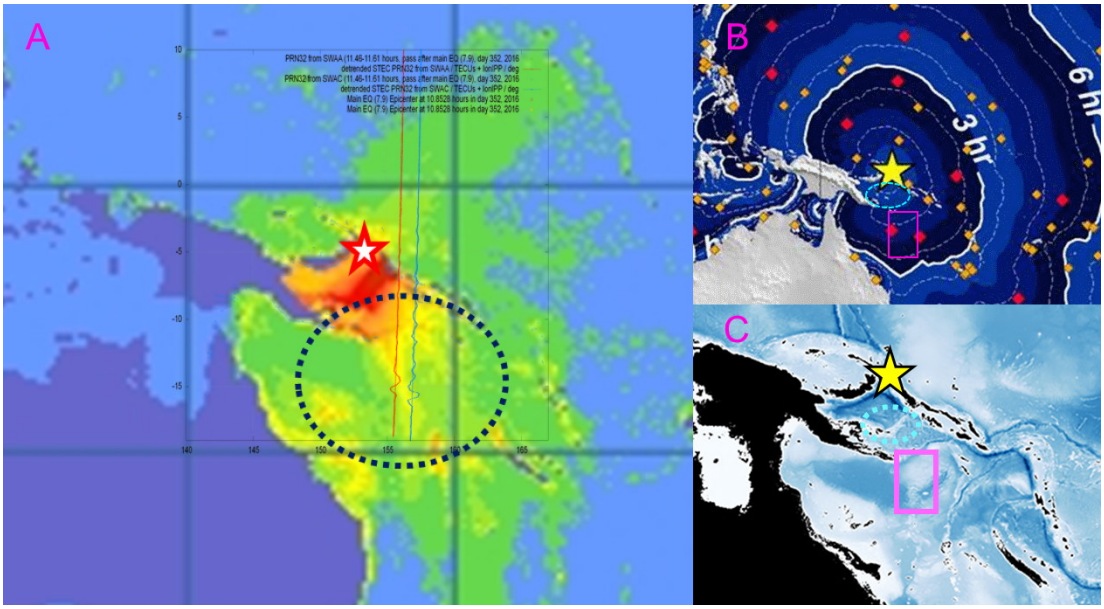

Fig. 6. A: The detrended VTEC overlapped on the trajectory of the ionospheric observing points regarding GPS satellite PRN 32 Swarm A & C, attached with the tsunami maximum amplitude graph, ranging from 0 (blue) to 100 cm (red), with intermediate growing values in green, yellow, and orange (source from [61]); B: Zoomed tsunami travel times, source from [61]; C: Zoomed Ocean Depth, white for the shallow part and blue for the deep sea (up to -8000 m in black), originating from the earth observatory of the U.S. NASA blue marble with topography and bathymetry, the yellow star for the epicentre, magenta rectangular for ionospheric observing points with higher detrended VTEC, and the cyan ellipse for the tsunami with the highest wave.

was here selected, because not all geometrical directions to GPS satellites can find disturbing signals similar to that in ED from LPs. This comparison was also suspected to show only an approximate similarity of signal PSD, however, the coincidence is better than expected. The three frequencies with high PSD at the start of the disturbance (approximately at 40 sec, 30 sec and 25 sec), become one lower frequency at the end, and are characteristic both in Figure 10 and Figure 11.

The main ED disturbing signal from Swarm C in Figure 12 occurred 45 min after Mw=7.9 EQ. It is even stronger in relation to that in Figure 10, and the corresponding selected topside TEC disturbance is also stronger as well (Figure 13). Both disturbances (Figure 12 and 13) have more periods that are disturbed, with respect to that observed in Figure 10 and Figure 11. The proximity of Swarm A and Swarm C may suggest that the situation has quickly evolved and disturbances have changed rapidly. Additionally, the similarity of PSD in Figure 12 and Figure 13 is again significant, although with different geometrical reference and kind of sensors. The coincidence of PSD from LPs and GNSS TEC confirms the ionospheric origin of the disturbances and excludes instrumental uncertainties. The observed chromatic spectra from two co-located Swarm LEOs (A and C) and from two different instruments (LP and GNSS POD receiver, figures 10,12,11,13), with a range of periods within [20,40]sec approximately, is in agreement with the above mentioned theory of [5].

C. Validation by Other Independent Measurements

Since the significant ionospheric disturbances from Swarm POD GNSS observation has been detected by PIES, and has been confirmed by means of Swarm A and C in-situ LP electron density (Ne) measurement, it will be validated by other independent measurements for the final issue of the PIES warning.

In this work, the ground GNSS dual-frequency data will be used as the additional sources of co-located ionospheric measurements. This is due to the fact that the DORIS and other LEO POD measurements were far from the epicenter during the event. The location of the employed ground GNSS receivers are shown in Figure 5B. Following the processing condition used for the Swarm POD GNSS data, the same spatial window with longitude of [140°E–167°E] and latitude of [19°S–10°N], and the time window of [10:00–12:00 UTC] are used for taking the ground GNSS data. The detrended STEC is done by the double time difference at 300 sec as the band pass filter which is able to reserve most components of the acoustic-gravity wave spectra [11]. Considering the coverage of ground GNSS observations to the potential circular waves, the GNSS ionospheric combination of specific station-satellites are selected for validating the PIES warning.

As a validation, in bottom plot of Figure 7 the keogram of detrended VTEC measurements from ground- and Swarm-based GNSS receivers is represented. This is done at the same time that the potential arrival times of the corresponding acoustic-gravity waves from the ground (assumed starting at E layer around 100 km, magenta dashed lines) and from the Swarm LEO (cyan dashed lines, assumed at the same Swarm height ($\sim$460 km), supported by the almost simultaneous impact on both in-situ ED provided by LP and in the VTEC of POD GNSS receiver, top plot of Figure 7), are represented. These results clearly show the compatible ionospheric response to the earthquake/tsunami at different heights.

After the mainshock, the wind field at the atmospheric

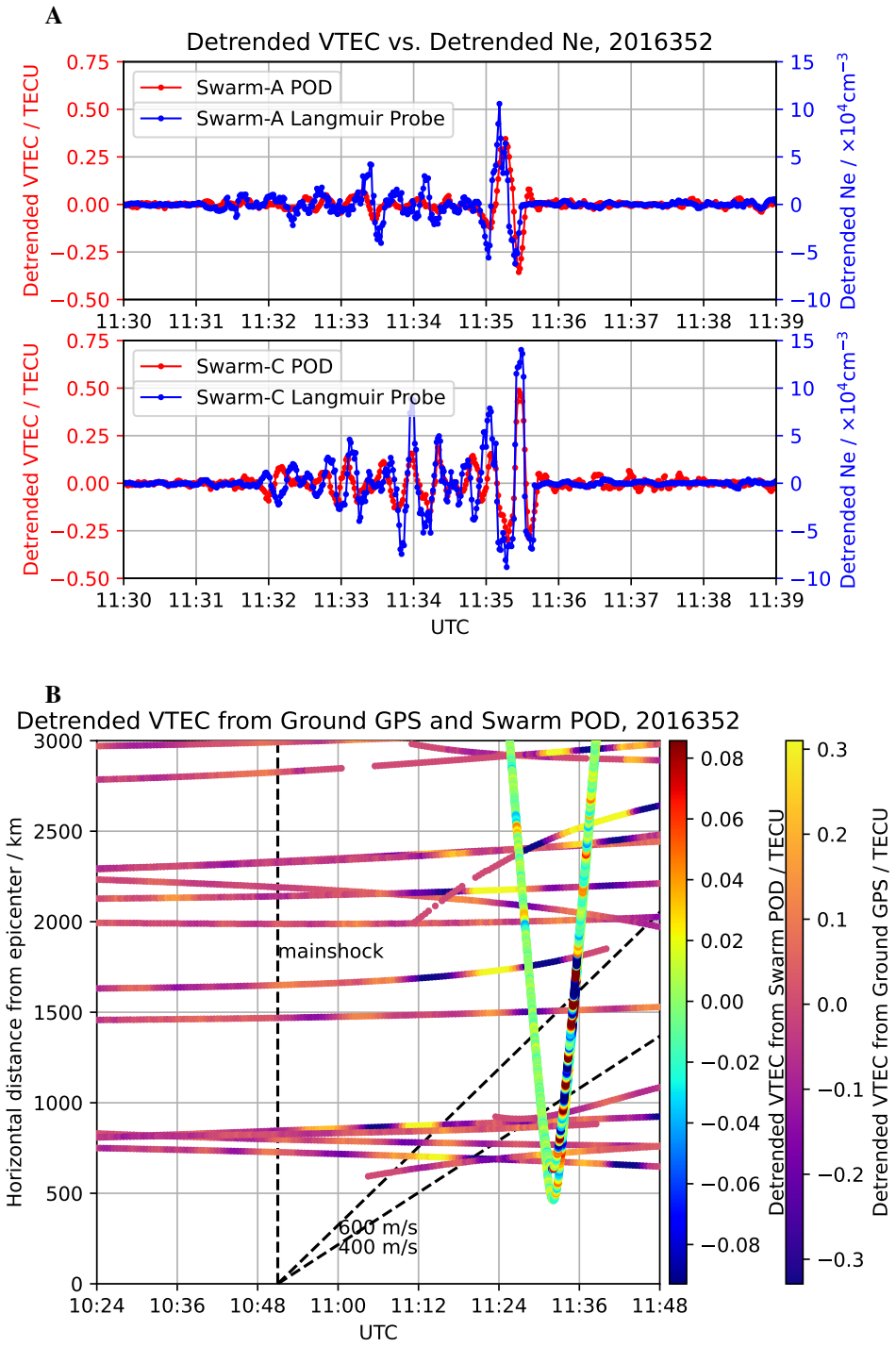

Fig. 7. A: Evolution vs time (x-axis) of detrended GNSS POD VTEC (red) and detrended LP electron density, Ne, (blue) for Swarm A (top subplot) and Swarm C (bottom plot) during the detection of the anomalous ionospheric disturbance after the PNG Mw7.9 earthquake (10h51m of day 352, 2016). B: Keogram of detrended VTEC from GNSS ground and POD Swarm receivers (Figure 5), right after PNG earthquake and coinciding with co-located Swarm pass.

pressure level of 1 hPa (at height of around 45 km) at 11:00 UTC shows the compatible disturbing level with two normal days, i.e. days 351 and 353 of 2016, see Figure 14. This wind field data show no extraordinary wind conditions. Moreover, there are no extraordinary rainfall conditions during these days. These would indicate that meteorological conditions do not affect the AGW propagation in the middle atmosphere [62].

V. 2016 Solomon Islands Event: Unexplained Pre-Seismic Ionospheric Signature with Swarm POD

As another case study for testing PIES, we found the Swarm LEO constellation approximately co-located in space

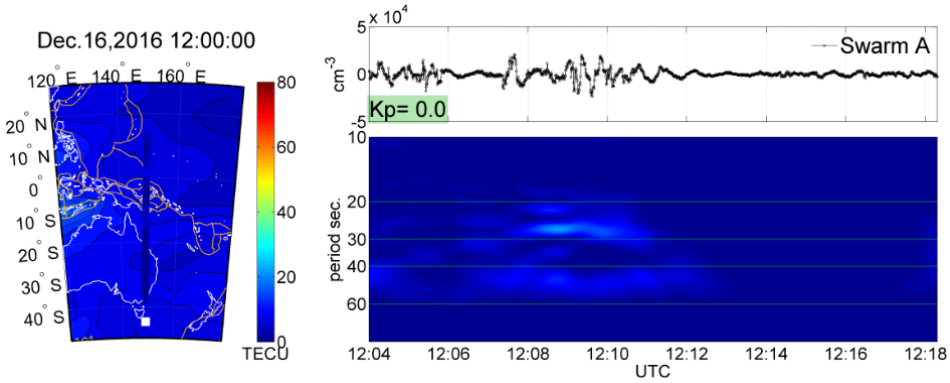

Fig. 8. Reference Swarm A high-pass filtered LP signal on December 16, 2016, at similar time of the day to disturbed signal on December 17. Top-right: high-pass filtered LP signal (50 sec) and *Kp* index. Bottom-right: STFT spectrogram of the above signal. Left: UQRG GIM with continents, tectonic plates and Swarm LP PSD sampled at period 40 sec.

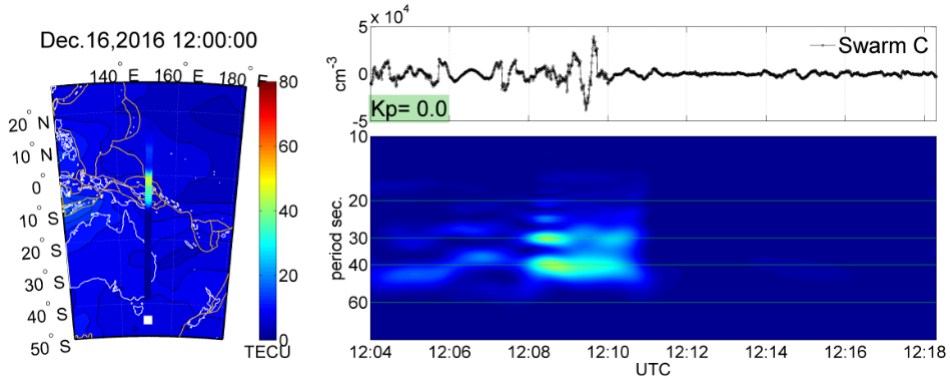

Fig. 9. The same as in Figure 8, but for Swarm C.

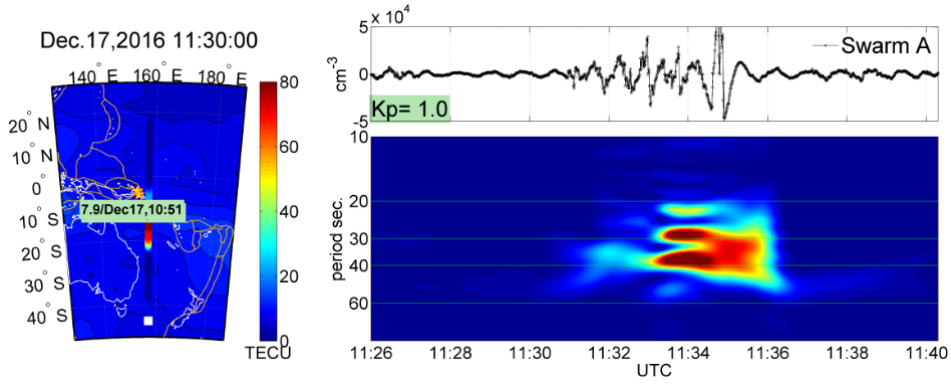

Fig. 10. Swarm A high-pass filtered LP signal on December 17, 2016, around 40 min after major EQ. Top-right: high-pass filtered LP signal (50 sec) and *Kp* index. Bottom-right: STFT spectrogram of the above signal. Left: UQRG GIM with continents, tectonic plates and Swarm LP PSD sampled at period 40 sec. White square denotes Swarm location in last epoch of the track.

and time with an earthquake and the driven tsunami occurred in the region of Solomon islands on 8 December 2016. The tracks of Swarm satellite B recorded the topside ionospheric disturbance regarding to the 17-days background disclosed by PIES at about a thousand kilometres west of the epicentre, and about 30 minutes before the main earthquake shock. The magnitude of this earthquake was 7.8. For the trajectories of the corresponding ionospheric observing points (in cyan points) vs. the epicentre (in red star) see Figure 15.

A. *PIES warning checking*

Following the application of PIES to the Swarm observations in Section 2, the ionospheric disturbances were extracted from the POD GPS receiver measurements, and processed with the same detrending time interval of 8 seconds. The detrended data showed the most significant value in the spatio-temporal window of 135°E–175°E vs. 40°S–10°N vs. 16:00-18:00 UTC (02:00-04:00 in local night), so to exclude far effects of the ionosphere. The elevation mask of $\geq 40^\circ$ was

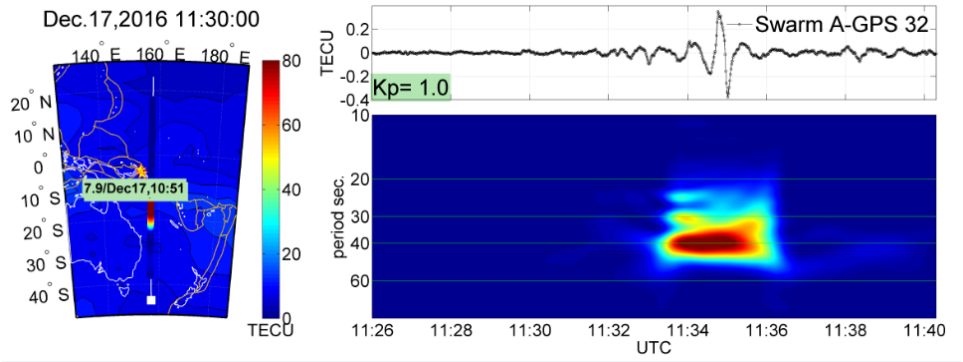

Fig. 11. Swarm A high-pass filtered topside TEC determined from Swarm A-GPS PRN 32 measurement on December 17, 2016, around 40 min after major EQ. Top-right: high-pass filtered LP signal (50 sec) and *Kp* index. Bottom-right: STFT spectrogram of the above signal. Left: UQRG GIM with continents, tectonic plates and Swarm TEC PSD sampled at period 40 sec. White square denotes Swarm location in last epoch of the track, white line is Swarm position with respect to colored GPS ionospheric observing points.

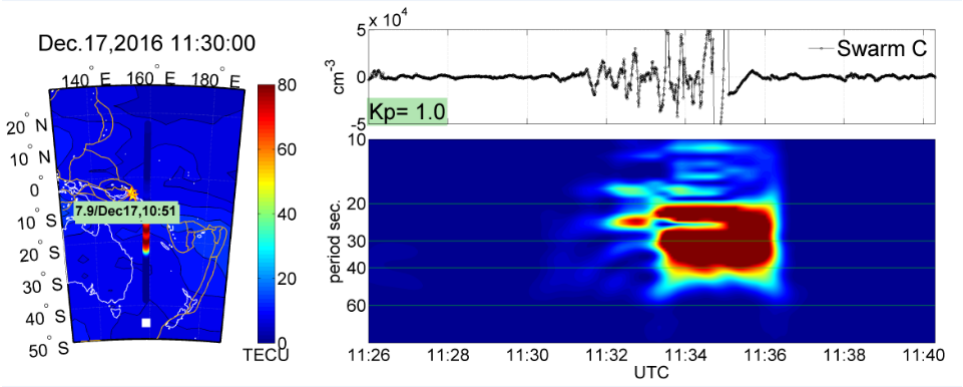

Fig. 12. The same as in Figure 10, but for Swarm C.

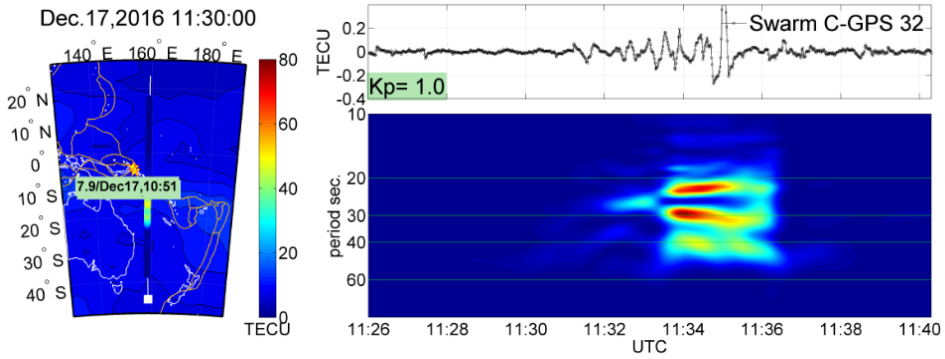

Fig. 13. The same as in Figure 11, but for Swarm C-GPS PRN 32 pair.

taken for decreasing the potential mapping error from STEC to VTEC. The geomagnetic equatorial index $Dst = -25$ nT [58], the planetary 3-hour-range index $Kp = 4$ [59], and the GOES X-ray flux measurement of Class-A [60] indicate the moderate space weather state, with no significant disturbances originated by these phenomena such as major solar activity, solar flare, or geomagnetic storm disturbances.

The detrended VTEC in Figure 16 shows that clear ionospheric disturbances, two times the next most negative one vs. the background of 17 days, occurred about 30 min before the earthquake (red vs green points), located at about one thousand kilometres west from the epicentre. The perturbation exhibits its maximum power at waves with a period of 16 sec. As it has been discussed above, and taking into account the high LEO velocity and expected ionospheric wavelengths, the actual period of the perturbation should be concentrated around 12-107 sec, see section IV-A. Similar to the case study in section IV-A, this significant disturbance (Figure 17A) was projected onto the horizontal trajectories of the ionospheric observing points regarding the corresponding Swarm satellite B, see

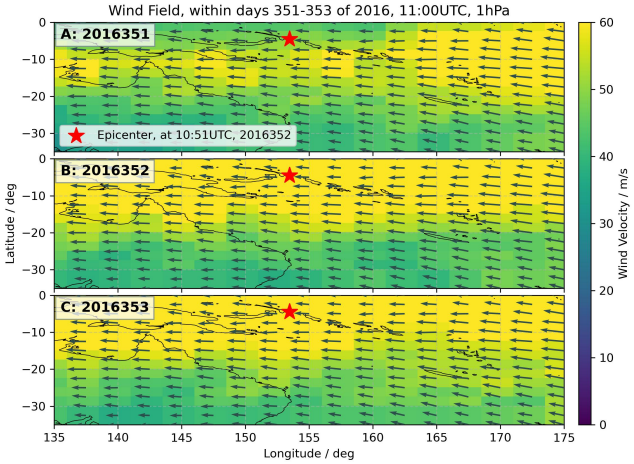

Fig. 14. Wind field at the atmospheric pressure level of 1 hPa, at 11:00 UTC, a), b) and c) respectively for the days 351, 352, and 353 of 2016 [62].

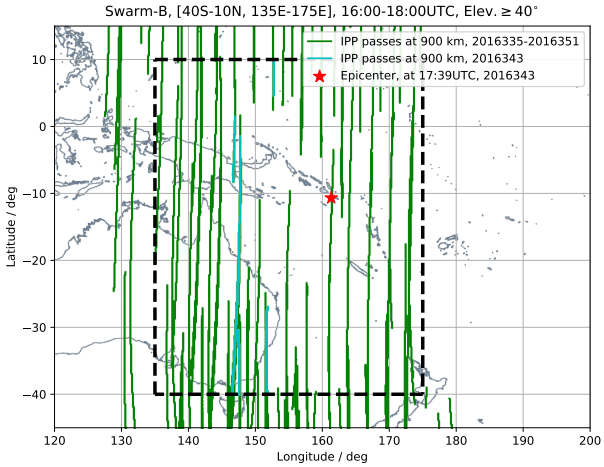

Fig. 15. Ionospheric observing points (in cyan) of Swarm B regarding GPS satellites within about 2 hour before the main shock of 2016 Solomon Island earthquake, at about a thousand kilometres west from epicentre, with a spatial window (135°E–175°E vs. 40°S–10°N), with a elevation mask of 40°. The green lines correspond to the observations for 16 adjacent normal days, with the same spatio-temporal window, and elevation mask as the earthquake day, and the red star for the epicentre.

Figure 17B. At about 17:11–17:12 UTC, the disturbances with the maximum energy locates about 1400 km southeast of the epicentre, corresponding to the detrended VTEC on the line of sight of Swarm satellite B and GPS satellite PRN 1. It is important to note that disturbance event in the form of waves occurring before the earthquake (not necessarily an earthquake precursor) is treated in a similar way than in the previous case, i.e., as a suspicious ionospheric PIES warning, which should be further verified with different types of measurements in the following sections, but regardless its interpretation, there is not consensus yet on the existence of potential earthquake ionospheric precursors, see different views in [63], [64], [65].

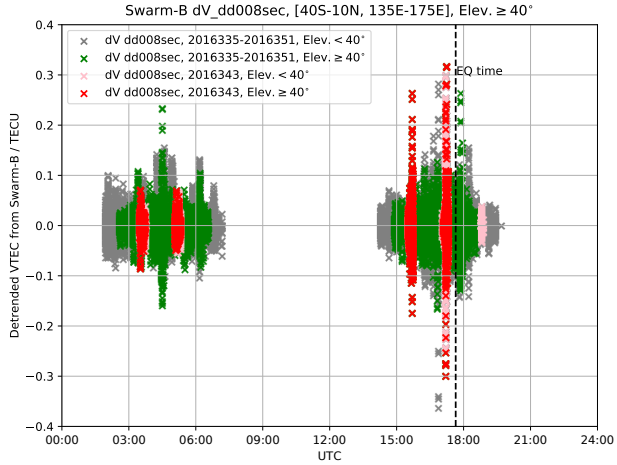

Fig. 16. Time evolution of detrended VTEC on the earthquake day (in red scatters), compared with 16 normal days with no earthquake record (in green scatters), the grey and pink points for the detrended VTEC with the elevation of less than 40 degree.

B. Validation by Power Spectra Analysis of Swarm B Langmuir Probe ED Data

The same kind of validation with the same parameters and respective scales has been performed for Swarm B trajectories applied in PIES detection of disturbing signals at the time of Mw=7.8 EQ on December 8, 2016. The selected Swarm B track was recorded on 8.12.2016, around 17:10 UTC, which is approximately 30 minutes before the largest Mw7.8 EQ in Solomon Islands region, occurred close to the western coast of San Cristobal island (17:38 UTC). Although the height of Swarm B is several tens of km larger than that of Swarm A and C, the high-pass filtering, the spectrograms and their sampling have been computed using exactly the same parameters, as for Swarm A/C pair in Section IV-B. The selection of DFT filtering period thresholds in this subsection and in Section IV-B, also aims to exclude low-frequency signals from sources other than seismic or tsunami sources, e.g. geomagnetic activity increase. The correctness of this threshold in our case can be confirmed to some extent in Figure 18, where at the time of increasing *Kp* index, no disturbance can be found, at least at the magnitude level analysed for the seismic-driven disturbances in Figure 19 and Figure 20 and previous figures. Figure 18 uses ED data from Swarm B LPs collected on the preceding reference day of December 7, 2016. The disturbance with respect to the common scale is almost invisible in the spectrogram in Figure 18 (bottom-right).

The situation changes markedly just before Mw=7.8 EQ on December 8. Figure 19 reveals an ED disturbance, which is somehow similar to those in Figure 10-13, as this disturbance occupies a large number of periods/frequencies with similarly large PSD. Figure 20 shows the corresponding selected topside TEC disturbance, where we see again some common features with the ED disturbance in Figure 19. The disturbance starts with one common amplitude at period >40 sec, with decreasing period. Then, the disturbance splits into two peaks around 30 sec (which are easier to spot in the TEC plot than in the

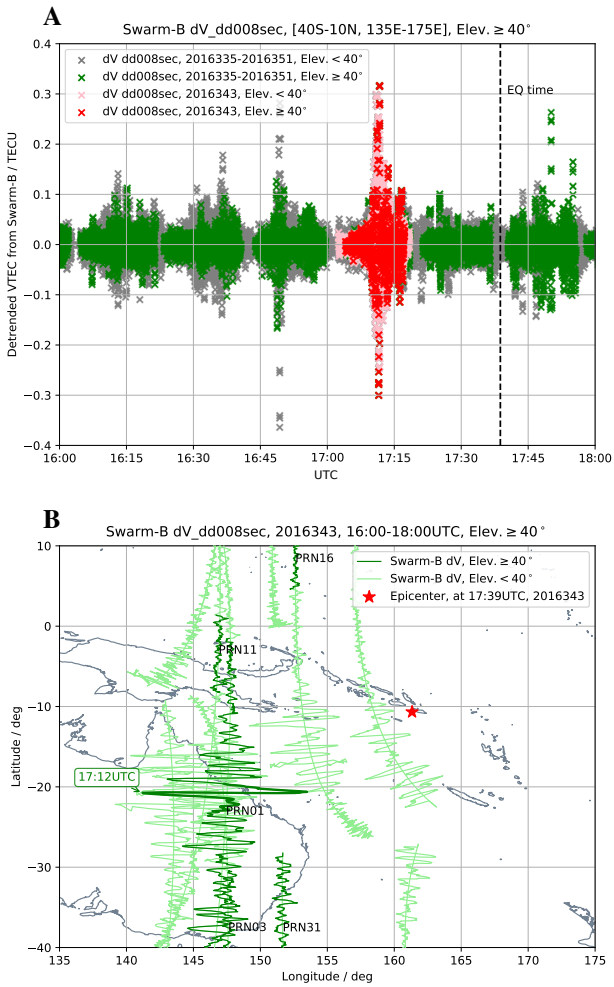

Fig. 17. A: Zoomed time evolution of detrended VTEC during 16:00–18:00 UTC, see Figure 16; B: The spatial evolution of detrended VTEC horizontally overlapping (0.1 TECU≡2 deg) the trajectories of ionospheric observing points regarding Swarm B are shown, the plots in green or light green respectively for the observation with elevation greater and lower than 40 degrees, the bold green plots for the detected maximum disturbances, the red star for the epicentre.

ED plot), and later on, into two disturbances around 20 sec period, which are better recognizable in the ED signal. This coincidence confirms the ionospheric origin of the disturbance, consistent as well with the most realistic non-monochromatic model of [5].

C. Validation by Other Independent Measurements

Besides the confirmation by study of Swarm B LP ED data, and due to the potential PIES warning, the validation has been complemented with two additional external sources of co-located ionospheric measurements: a) ground GNSS dual-frequency measurements, and b) DORIS dual-frequency measurements. The location of the employed ground GNSS receivers, the ground DORIS transmitters and the LEO-on-board DORIS receivers are shown in Figure 21.

Regarding the DORIS dual-frequency measurement, the data processing has been done by the multi-TOMION model [41]. The mapping function is assumed at an effective height of 450 km regarding the disturbances, which is lower than the one assumed over the Swarm satellites for the LEO-based GPS measurements. In addition, the double difference with the time step of 20 sec is used to derive the ionospheric disturbances taking into account the receiver-transmitter velocity and wavelength.

With the same processing condition used for the LEO GNSS data, i.e. the spatial window with longitude of [135°E–175°E] and latitude of [40°S–10°N], the temporal window of the time period [16:00–18:00 UTC] and the elevation mask of greater than $40°$, the detrended VTEC, including the ionospheric disturbances around the passes, of the LEO DORIS receivers on the earthquake day is shown in Figure 22. Note that the time series showing the disturbances of increasing intensity (marked in purple in Figure 22) at time about 16:43–16:45 UTC (02:43-04:45 in local night) is of interest. Following the steps of PIES, the DORIS data with the 14 neighbouring days are also studied by mean of the same spatio-temporal window and the elevation mask, their time series (in green) are organized in Figure 22, as well as the one (in red) on the earthquake day. The perturbation on detrended VTEC on the earthquake day occurred about 55 min before the earthquake, showing significantly larger intensity than the ones in the normal days, which locates at the southeast of the epicentre. In comparison to the significant disturbance measured by Swarm B, the detected disturbances might be compatible in terms of their time location (less than 30 minutes apart) and their latitudes, although they are about 2500 km away.

The GNSS ground stations for validation were selected from the permanent GNSS networks, i.e. the Australian CORS (AUSCORS), Land Information New Zealand (LINZ), and the IGS network. Besides the TOMION model, the double time difference with two time steps at 60 and 300 sec are used to find the earthquake signal in the ionosphere (see [11]), and the same spatio-temporal window than the case for Swarm satellite observation. Note a smaller elevation mask of 10° is applied to look for the potential TIDs occurring above the ocean, see the previous case study [11]. In addition, the ionospheric effective height regarding ground GNSS is set as 250 km for studying the ionospheric disturbances lower than F layer, see the detailed explanation in [18]. By means of the double difference with a time step of 300 sec, the results of the detrended VTEC preserve a stronger intensity than that of 60 sec. Since about 17:00 UTC, the results of 300 sec show the most significant disturbances compared with the ones of normal days, see Figure 23A. The disturbances occurring about 3-10 minutes before the peak disturbance of Swarm-B, see Figure 23B, come from a region with longitude of [155°E–158°E] and latitude of [23°S–20°S] which locates east of Swarm-B and also southwest of the epicentre.

The original observation shown in Figure 24A, i.e. the GNSS ionospheric combination L_I including such disturbances, were arbitrarily aligned along the time sequence of the STEC decrease. Considering the locations of GNSS receivers in Figure 24B, the results clearly show a group of ionospheric disturbances manifested as a ”N-shape” with intensities of 2 TECUs, propagating from southeast to northwest (i.e. approximately perpendicular to the EQ epicentre direction)

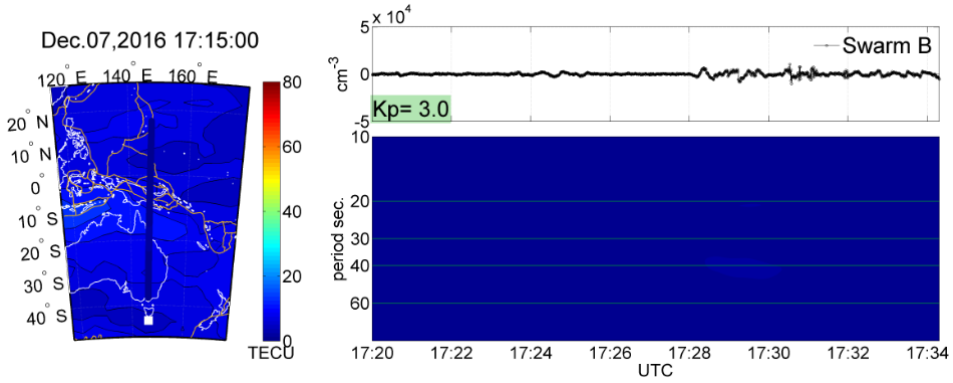

Fig. 18. Reference Swarm B high-pass filtered LP signal on December 7, 2016, at similar time of the day to disturbed signal on December 8. Top-right: high-pass filtered LP signal (50 sec) and *Kp* index. Bottom-right: STFT spectrogram of the above signal. Left: UQRG GIM with continents, tectonic plates and Swarm LP PSD sampled at period 40 sec.

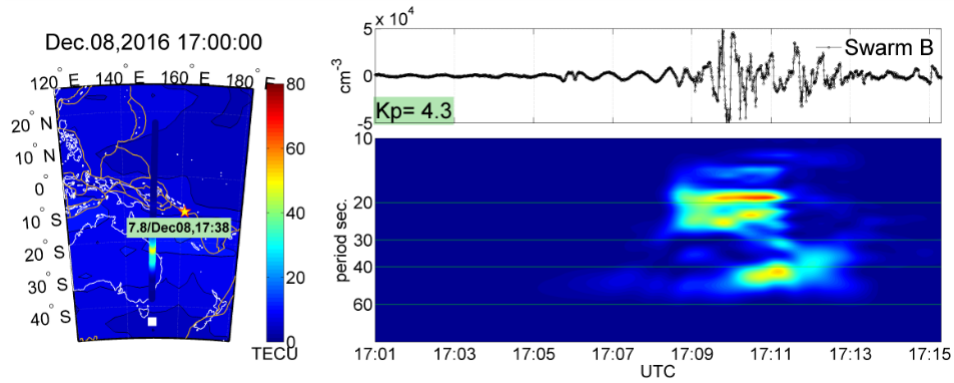

Fig. 19. Swarm B high-pass filtered LP signal on December 8, 2016, around 30 min before major EQ. Top-right: high-pass filtered LP signal (50 sec) and *Kp* index. Bottom-right: STFT spectrogram of the above signal. Left: UQRG GIM with continents, tectonic plates and Swarm LP PSD sampled at period 40 sec.

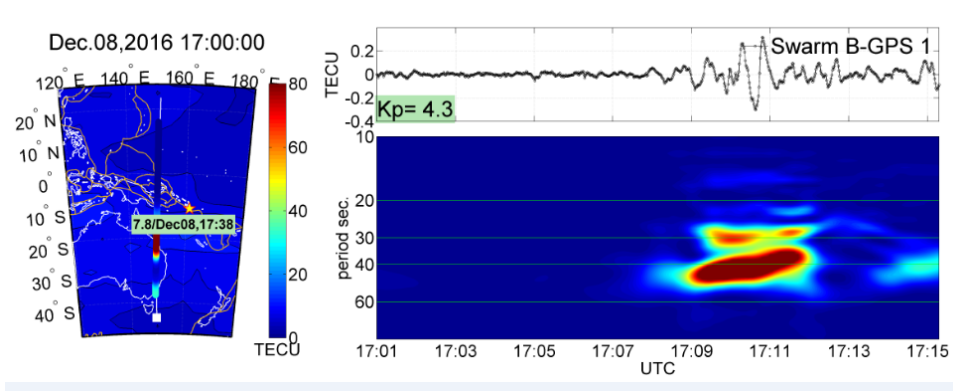

Fig. 20. The same parameters as in Figure 19, but for topside TEC determined from Swarm B-GPS PRN 1 measurement.

with a propagation velocity of about 230-270 m/s, and a raw wavelength estimation of about 400-600 km. Note that the ”N-shape” TEC depletion shows much slower variation than the typical ionospheric response to the large/middle magnitude earthquakes [11]. Figure 25 shows the ionospheric disturbances derived from multiple measurements at different locations and heights. The ionospheric disturbances were detected for the first time from the DORIS observation data (i.e. the ionospheric observing points regarding NOXB-JA2 pair, at 16:44UTC), taken into account the estimated velocity and azimuth of propagation. The next occurrence is from ground-based GNSS measurements during 17:02-17:12, followed by measurements from Swarm-B POD-GNSS. The disturbances are shown both at the topside ionosphere (by Swarm) and at the lower ionosphere (by DORIS). The ionospheric disturbances appearing along the time and distance sequence is evident, as a TEC depletion and the afterward fluctuations, see Figure 25. In summary, the results by ground stations show the

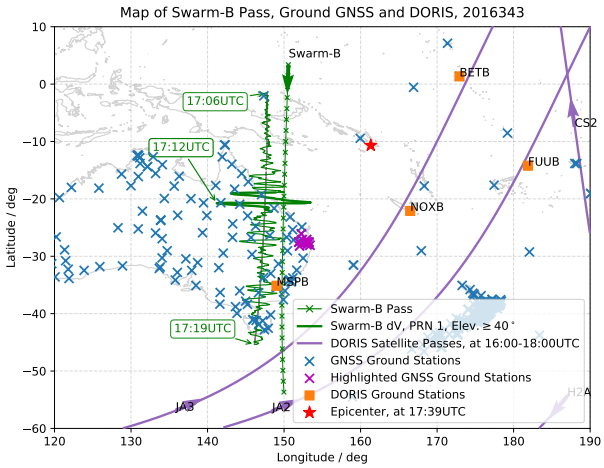

Fig. 21. Location and passes of measurements, the green line with marks for the trajectory of Swarm B, the green line for the detrended VTEC projected onto the passes of the ionospheric observing points regarding Swarm-B and GPS satellite PRN 1 with greater than 40° elevation, the bold green line for the detrended VTEC with maximum energy, the purple line for passes of LEO-on-board DORIS receivers, blue marks for GNSS ground stations, magenta marks for GNSS ground stations which detected significant disturbances on the EQ day in particular, and orange rectangular for ground DORIS transmitters.

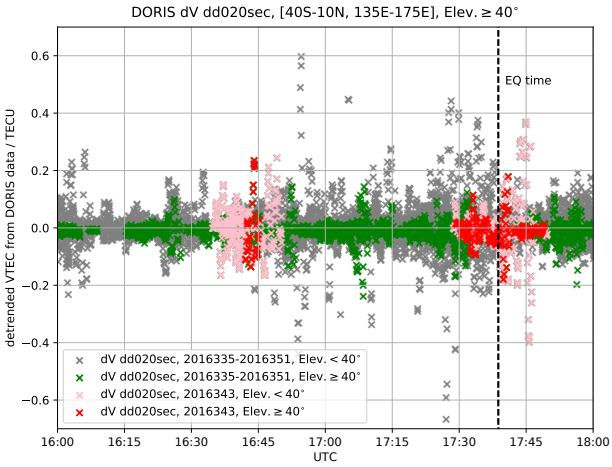

Fig. 22. Detrended VTEC of DORIS measurement during 16:00-18:00 on the earthquake day (in red), with a spatial window of [135°E–175°E vs. 40°S–10°N], compared with the adjacent days 335 to 351 of 2016 (in green), the observations with elevation of lower than 40° have been respectively marked by pink and grey.

consistency of the ionospheric perturbation detection in time and location with of Swarm satellite B.

Finally, on the earthquake day, the wind field at the atmospheric pressure level of 1 hPa (at height of ∼45 km) at 17:00 UTC shows the compatible disturbing level with two normal days, i.e. days 342 and 344 of 2016, see Figure 26, which are sourced from [62], showing no extraordinary wind conditions. Moreover, there are no extraordinary rainfall conditions during these days.

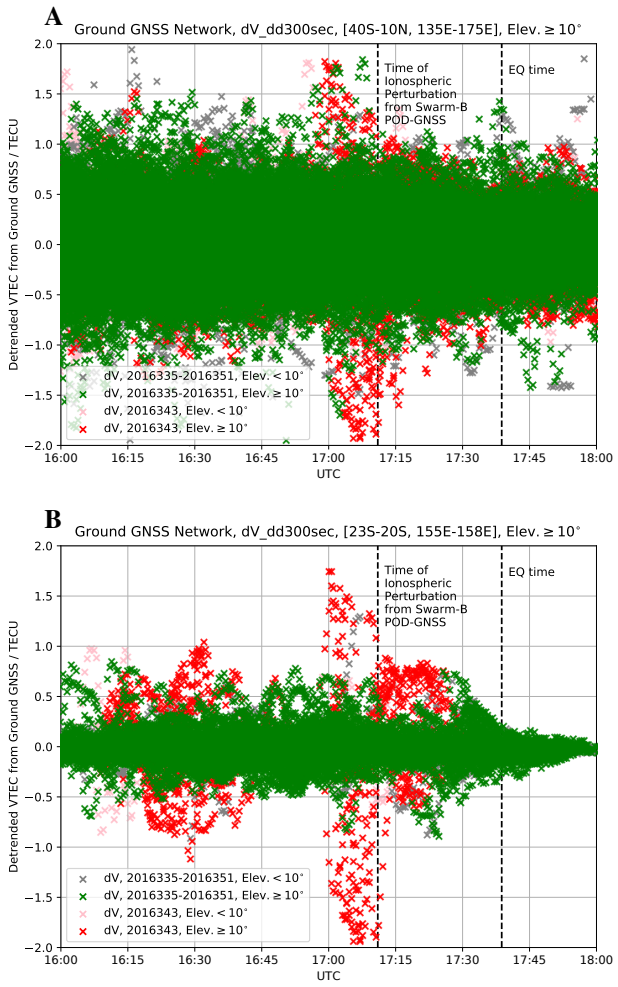

Fig. 23. A: Detrended VTEC of Ground GNSS measurement by double difference with time step of 300 sec, during 16:00-18:00 on the earthquake day (in red), with a spatial window of [135°E–175°E, 40°S–10°N], compared with the adjacent days 335 to 351 of 2016 (in green), the observations with elevation of lower than 10° have been respectively marked by pink and grey. B: the same as A with a zoomed spatial window of [155°E–158°E, 23°S–20°S].

VI. Conclusions

We have presented the POD-GNSS LEO Detrended Ionospheric Electron Content Significant Deviations (PIES), a method to detect the significant ionospheric disturbances from the detrended total electron content of the GNSS POD LEO data, which can help in particular to identify the tsunami signatures in the topside ionosphere-based observations. The results are validated by other independent measurements. This method relying on the ongoing and historic POD GNSS measurements, could be an effective tool for contributing to potential warning of earthquakes and tsunamis based solely on LEO satellites. By analysing POD-GNSS data from Swarm LEO satellites with PIES, the topside ionospheric activities during two earthquake and tsunami cases in PNG region in 2016 are studied. And the anomalous ionospheric disturbances in the spectral ranges of tsunami-related gravity waves and earthquake-related acoustic waves are identified thanks to the collocated Swarm LEO data and validated vs. other sources.

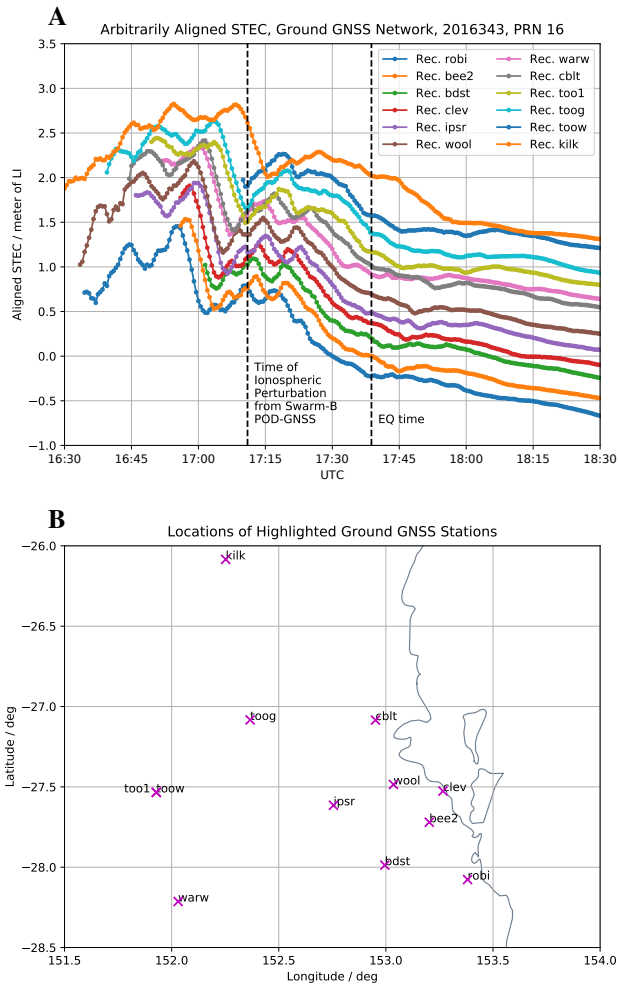

Fig. 24. A: Time evolution of the arbitrarily aligned slant TECs, for the GPS satellite PRN 16, at the time of 16:30–18:50, the color codes of lines correspond to different GNSS receivers, the black dash line indicates the time of the earthquake at 17:39 UTC; B: Locations of regarding ground GNSS stations.

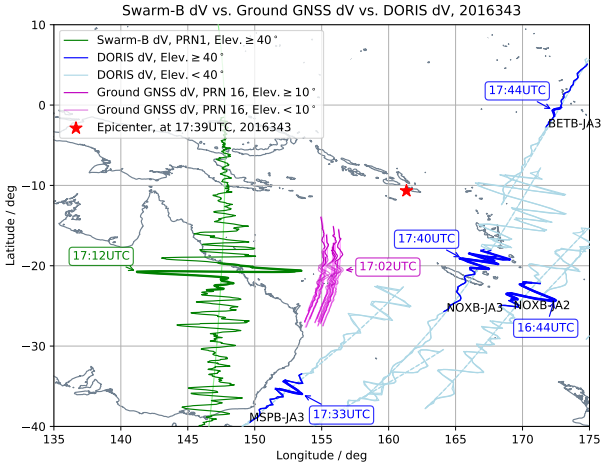

Fig. 25. Detrended VTEC comparison between results of Swarm-B, of Ground GNSS and of DORIS. The green line for the detrended VTEC projected onto the ionospheric observing points of GPS satellites PRN 1 from Swarm-B and with the elevation mask of 40°, the blue line for the detrended VTEC projected onto the passes of the light of sights regarding ground transmitters and all LEO receivers, the purple line for the detrended VTEC projected onto the observing points regarding highlighted ground GNSS receivers and GPS satellite PRN 16, the light blue and light purple respectively for the ones with less than 40° and 10°, respectively, the bold green, bold blue and bold purple lines for the respective series of detrended VTEC with maximum energies.

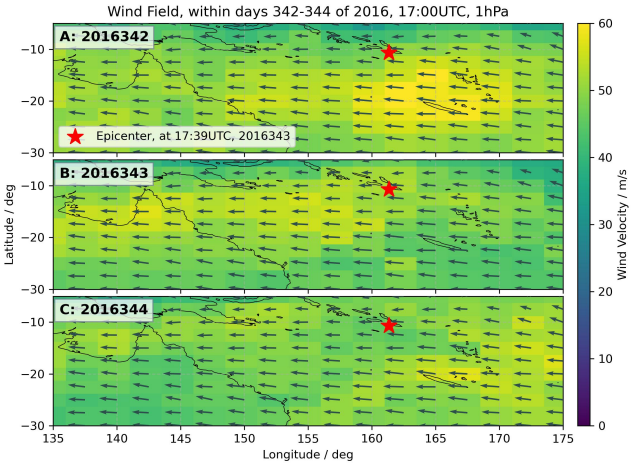

Fig. 26. Wind field at the atmospheric pressure level of 1 hPa, at 17:00 UTC, a), b) and c) respectively for the days 342, 343, and 344 of 2016 [62].

The likely origin of the tsunami to explain part of the observed anomalous ionospheric signals has been determined thanks as well to a novel comparison of the required vertical velocity of the potential gravity wave associated with the tsunami. Indeed it is consistent with the most-recent theory [5] which shows that a tsunami (which is localized in space and time) excites a spectrum of gravity waves, some of which have faster horizontal phase speeds than the tsunami. These fast gravity waves also have very high vertical phase speeds (up to 300 m/s). Our results, however, are not consistent with previous model works which considered the tsunami as a monochromatic ocean wave (not localized in space and time). In other words, this work can be considered as well as a possible experimental confirmation of the most recent and realistic model of gravity wave propagation, in particular in the ionosphere.

It is also important to emphasize, in the context of the validation of PIES results, the analysis of spectral responses in LP ED signals on board Swarm A and Swarm B, detects many ED disturbances that are coincident with persistent seismic activity in December 2016 in PNG and Solomon Islands regions. Such analysis is in good agreement with the results provided by the independent POD GNSS data. The samples of ED power spectrum at frequencies corresponding to 350-450 km along orbital arcs, show coincidence of large spectral peaks with critical seismic activity, like first or largest earthquakes in the region, and coincidence of low spectrum responses with the relaxation time. Similar spectral representations of disturbing signals in LP ED data are found several times, which is promising for the future spectral analysis for the recognition of different disturbing signals in the ionosphere.

Regarding to the PNG Mw 7.9 earthquake, the presented results can help to open a new door in the applicability of LEO POD GNSS data to contribute in the real-time LEO tsunami detection and monitoring thanks to the increasing number of GNSS LEO receivers as potential ionospheric sounders on board of hundreds of cubesats.

In the case of the ionospheric disturbances found before the Solomon Mw 7.8 earthquake, the highly suspicious PIES warning might enlarge the potential application of the indicator in such LEO earthquake/tsunami monitoring, which does not necessarily have to be a definite earthquake precursor warning.

Using the PIES methodology, in the passes around 30 minutes before the earthquake, an unexplained disturbance signal of about 16 seconds period, was found in the detrended VTEC (considering only elevations above 40 degrees to minimise errors in the mapping function). This detection was done by the analysis of POD GNSS Swarm constellation data during 17 days in the region around the earthquake and tsunami held at Solomon islands. This result, unexplained so far, has been confirmed with independent LP electron density, DORIS and ground-based GNSS measurements.

The use of both ground-based data, i.e. GNSS receivers displacements near the epicentre of an earthquake, as well as the ionospheric signature of earthquakes and tsunami in their data, can provide (a) the validation of the proposed method to also help establish the occurrence and intensity of an earthquake soon after it happens; and (b) a means to develop further the technique for processing the GNSS data from artificial satellite receivers to detect in particular tsunamis from orbits higher than 450km.

The future work can include to adapt the overall PIES strategy used in PNG earthquake/tsunami and in Solomon Island earthquake for real time or nearly real time computation and analysis.

ACKNOWLEDGMENT

This work has been partially supported by the COSTO ESA-funded project (ESA ITT AO/1-9514/18/NL/IA). Also it was partially supported by the 2017 SGR-0851 grant of the Generalitat de Catalunya and by the EU project 101007599 - PITHIA-NRF. The data for this paper are available and they can be requested from H. Yang (h.yang@upc.edu) and M. Hernández-Pajares (manuel.hernandez@upc.edu).

REFERENCES

[1] W. Peltier and C. Hines, "On the possible detection of tsunamis by a monitoring of the ionosphere," *Journal of Geophysical Research*, vol. 81, no. 12, pp. 1995–2000, 1976.

[2] G. Occhipinti, P. Lognonné, E. A. Kherani, and H. Hébert, "Three-dimensional waveform modeling of ionospheric signature induced by the 2004 sumatra tsunami," *Geophysical research letters*, vol. 33, no. 20, 2006.

[3] M. P. Hickey, G. Schubert, and R. Walterscheid, "Propagation of tsunami-driven gravity waves into the thermosphere and ionosphere," *Journal of Geophysical Research: Space Physics*, vol. 114, no. A8, 2009.

[4] J. Makela, P. Lognonné, H. Hébert, T. Gehrels, L. Rolland, S. Allgeyer, A. Kherani, G. Occhipinti, E. Astafyeva, P. Coïsson *et al.*, "Imaging and modeling the ionospheric airglow response over hawaii to the tsunami generated by the tohoku earthquake of 11 march 2011," *Geophysical Research Letters*, vol. 38, no. 24, 2011.

[5] S. L. Vadas, J. J. Makela, M. J. Nicolls, and R. F. Milliff, "Excitation of gravity waves by ocean surface wave packets: Upward propagation and reconstruction of the thermospheric gravity wave field," *Journal of Geophysical Research: Space Physics*, vol. 120, no. 11, pp. 9748–9780, 2015.

[6] X. Meng, P. Vergados, A. Komjathy, and O. Verkhoglyadova, "Upper atmospheric responses to surface disturbances: An observational perspective," *Radio Science*, vol. 54, no. 11, pp. 1076–1098, 2019.

[7] C. Hines, "Gravity waves in the atmosphere," *Nature*, vol. 239, no. 5367, pp. 73–78, 1972.

[8] M. Pitteway and C. Hines, "The viscous damping of atmospheric gravity waves," *Canadian Journal of Physics*, vol. 41, no. 12, pp. 1935–1948, 1963.

[9] S. L. Vadas, "Horizontal and vertical propagation and dissipation of gravity waves in the thermosphere from lower atmospheric and thermospheric sources," *Journal of Geophysical Research: Space Physics*, vol. 112, no. A6, 2007.

[10] M. Hernández-Pajares, J. M. Juan, J. Sanz, À. Aragón-Àngel, A. García-Rigo, D. Salazar, and M. Escudero, "The ionosphere: effects, GPS modeling and the benefits for space geodetic techniques," *Journal of Geodesy*, vol. 85, no. 12, pp. 887–907, 2011.

[11] H. Yang, E. Monte-Moreno, and M. Hernández-Pajares, "ADDTID: An alternative tool for studying earthquake/tsunami signatures in the ionosphere. Case of the 2011 Tohoku earthquake," *Remote Sensing*, vol. 11, no. 16, p. 1894, 2019.

[12] M. Hernández-Pajares, J. Juan, J. Sanz, R. Orus, A. Garcia-Rigo, J. Feltens, A. Komjathy, S. Schaer, and A. Krankowski, "The IGS VTEC maps: a reliable source of ionospheric information since 1998," *Journal of Geodesy*, vol. 83, no. 3-4, pp. 263–275, 2009.

[13] J. Artru, V. Ducic, H. Kanamori, P. Lognonné, and M. Murakami, "Ionospheric detection of gravity waves induced by tsunamis," *Geophysical Journal International*, vol. 160, no. 3, pp. 840–848, 2005.

[14] A. Komjathy, D. Galvan, P. Stephens, M. Butala, V. Akopian, B. Wilson, O. Verkhoglyadova, A. Mannucci, and M. Hickey, "Detecting ionospheric tec perturbations caused by natural hazards using a global network of gps receivers: The tohoku case study," *Earth, planets and space*, vol. 64, no. 12, pp. 1287–1294, 2012.

[15] G. Occhipinti, L. Rolland, P. Lognonné, and S. Watada, "From sumatra 2004 to tohoku-oki 2011: The systematic gps detection of the ionospheric signature induced by tsunamigenic earthquakes," *Journal of Geophysical Research: Space Physics*, vol. 118, no. 6, pp. 3626–3636, 2013.

[16] I. Azeem, S. L. Vadas, G. Crowley, and J. J. Makela, "Traveling ionospheric disturbances over the united states induced by gravity waves from the 2011 tohoku tsunami and comparison with gravity wave dissipative theory," *Journal of Geophysical Research: Space Physics*, vol. 122, no. 3, pp. 3430–3447, 2017.

[17] J. Liu, Y. Tsai, S. Chen, C. Lee, Y. Chen, H. Yen, W. Chang, and C. Liu, "Giant ionospheric disturbances excited by the m9. 3 sumatra earthquake of 26 december 2004," *Geophysical Research Letters*, vol. 33, no. 2, 2006.

[18] M. Hernández-Pajares, J. Juan, and J. Sanz, "Medium-scale traveling ionospheric disturbances affecting GPS measurements: Spatial and temporal analysis," *Journal of Geophysical Research: Space Physics (1978–2012)*, vol. 111, no. A7, 2006.

[19] Y.-M. Yang, X. Meng, A. Komjathy, O. Verkholyadova, R. Langley, B. Tsurutani, and A. Mannucci, "Tohoku-oki earthquake caused major ionospheric disturbances at 450 km altitude over alaska," *Radio Science*, vol. 49, no. 12, pp. 1206–1213, 2014.

[20] A. Komjathy, Y.-M. Yang, X. Meng, O. Verkhoglyadova, A. J. Mannucci, and R. B. Langley, "Recent developments in understanding natural-hazards-generated tec perturbations: Measurements and modeling results," in *the Proceedings of the 2015 Ionospheric Effects Symposium, Alexandria, VA, May*, 2015, pp. 12–14.

[21] W. Jarmolowski, P. Wielgosz, A. Krypiak-Gregorczyk, B. Milanowska, and R. Haagmans, "Seismic ionospheric disturbances related to Chile-Illapel 2015 earthquake and tsunami observed by Swarm and ground GNSS stations," in *EGU General Assembly 2021*, vol. EGU21-8218. online, 19–30 Apr 2021: Springer, 2021.

[22] M. Schmidt, A. Goss, and E. Erdogan, "Monitoring and Modelling of ionospheric disturbances by means of GRACE, GOCE and Swarm in-situ observations," in *EGU General Assembly 2021*, vol. EGU21-14214. online, 19–30 Apr 2021: Springer, 2021.

[23] S.-C. Han, J. Sauber, and R. Riva, "Contribution of satellite gravimetry to understanding seismic source processes of the 2011 tohoku-oki earthquake," *Geophysical Research Letters*, vol. 38, no. 24, 2011.

[24] M. J. Fuchs, J. Bouman, T. Broerse, P. Visser, and B. Vermeersen, "Observing coseismic gravity change from the japan tohoku-oki 2011 earthquake with goce gravity gradiometry," *Journal of Geophysical Research: Solid Earth*, vol. 118, no. 10, pp. 5712–5721, 2013.

[25] P. Coïsson, P. Lognonné, D. Walwer, and L. M. Rolland, "First tsunami gravity wave detection in ionospheric radio occultation data," *Earth and Space Science*, vol. 2, no. 5, pp. 125–133, 2015.

[26] R. F. Garcia, E. Doornbos, S. Bruinsma, and H. Hebert, "Atmospheric gravity waves due to the Tohoku-Oki tsunami observed in the thermosphere by GOCE," *Journal of Geophysical Research: Atmospheres*, vol. 119, no. 8, pp. 4498–4506, 2014.

[27] D. A. Galvan, A. Komjathy, M. P. Hickey, P. Stephens, J. Snively, Y. T. Song, M. D. Butala, and A. J. Mannucci, "Ionospheric signatures of tohoku-oki tsunami of march 11, 2011: Model comparisons near the epicenter," *Radio Science*, vol. 47, no. 4, 2012.

[28] M. Lee, R. Pradipta, W. Burke, A. Labno, L. Burton, J. Cohen, S. Dorfman, A. Coster, M. Sulzer, and S. Kuo, "Did tsunami-launched gravity waves trigger ionospheric turbulence over arecibo?" *Journal of Geophysical Research: Space Physics*, vol. 113, no. A1, 2008.

[29] M. Kamogawa, Y. Orihara, C. Tsurudome, Y. Tomida, T. Kanaya, D. Ikeda, A. R. Gusman, Y. Kakinami, J.-Y. Liu, and A. Toyoda, "A possible space-based tsunami early warning system using observations of the tsunami ionospheric hole," *Scientific reports*, vol. 6, no. 1, pp. 1–7, 2016.

[30] A. Komjathy, Y.-M. Yang, X. Meng, O. Verkhoglyadova, A. J. Mannucci, and R. B. Langley, "Detection of natural-hazards-generated tec perturbations using ground-based and spaceborne ionospheric measurements and potential new applications," in *Proceedings of the ION 2015 Pacific PNT Meeting*, 2015, pp. 522–527.

[31] A. De Santis, D. Marchetti, F. J. Pavón-Carrasco, G. Cianchini, L. Perrone, C. Abbattista, L. Alfonsi, L. Amoruso, S. A. Campuzano, M. Carbone *et al.*, "Precursory worldwide signatures of earthquake occurrences on swarm satellite data," *Scientific reports*, vol. 9, no. 1, pp. 1–13, 2019.

[32] G. Olivares-Pulido, M. Hernández-Pajares, A. Aragón-Àngel, and A. García-Rigo, "A linear scale height Chapman model supported by GNSS occultation measurements," *Journal of Geophysical Research: Space Physics*, vol. 121, no. 8, pp. 7932–7940, 2016.

[33] F. d. S. Prol, D. R. Themens, M. Hernández-Pajares, P. d. O. Camargo, and M. T. d. A. H. Muella, "Linear vary-chap topside electron density model with topside sounder and radio-occultation data," *Surveys in Geophysics*, vol. https://doi.org/10.1007/s10712-019-09521-3, pp. 1–17, 2019.

[34] M. Hernández-Pajares, M. Garcia-Fernàndez, A. Rius, R. Notarpietro, A. von Engeln, G. Olivares-Pulido, À. Aragón-Àngel, and A. García-Rigo, "Electron density extrapolation above f2 peak by the linear vary-chap model supporting new global navigation satellite systems-leo occultation missions," *Journal of Geophysical Research: Space Physics*, vol. 122, no. 8, pp. 9003–9014, 2017.

[35] H. Lyu, M. Hernández-Pajares, E. Monte-Moreno, and E. Cardellach, "Electron density retrieval from truncated radio occultation gnss data," *Journal of Geophysical Research: Space Physics*, vol. 124, no. 6, pp. 4842–4851, 2019.

[36] V. V. Forsythe, T. Duly, D. Hampton, and V. Nguyen, "Validation of ionospheric electron density measurements derived from spire cubesat constellation," *Radio Science*, vol. 55, no. 1, p. e2019RS006953, 2020.

[37] M. J. Angling, O. Nogués-Correig, V. Nguyen, S. Vetra-Carvalho, F.-X. Bocquet, K. Nordstrom, S. E. Melville, G. Savastano, S. Mohanty, and D. Masters, "Sensing the ionosphere with the spire radio occultation constellation," *Journal of Space Weather and Space Climate*, vol. 11, p. 56, 2021.

[38] K. Wang, A. Allahvirdi-Zadeh, A. El-Mowafy, and J. N. Gross, "A sensitivity study of pod using dual-frequency gps for cubesats data limitation and resources," *Remote Sensing*, vol. 12, no. 13, p. 2107, 2020.

[39] W. Jarmołowski, A. Belehaki, M. H. Pajares, M. Schmidt, A. Goss, P. Wielgosz, H. Yang, A. Krypiak-Gregorczyk, I. Tsagouri, E. Paouris, E. Monte-Moreno, A. García-Rigo, B. Milanowska, E. Erdogan, V. Graffigna, and R. Haagmans, "Combining swarm langmuir probe observations, leo-pod-based and ground-based gnss receivers and ionosondes for prompt detection of ionospheric earthquake and tsunami signatures: case study of 2015 chile-illapel event," pp. 1–28, 2021.

[40] J. van den IJssel, J. Encarnação, E. Doornbos, and P. Visser, "Precise science orbits for the swarm satellite constellation," *Advances in Space Research*, vol. 56, no. 6, pp. 1042–1055, 2015.

[41] M. Hernández-Pajares, H. Lyu, M. Garcia-Fernandez, and R. Orus-Perez, "A new way of improving global ionospheric maps by ionospheric tomography: consistent combination of multi-gnss and multi-space geodetic dual-frequency measurements gathered from vessel-, leo- and ground-based receivers," *Journal of Geodesy*, vol. 94, no. 8, pp. 1–16, 2020.

[42] N. Perevalova, V. Sankov, E. Astafyeva, and A. Zhupityaeva, "Threshold magnitude for ionospheric TEC response to earthquakes," *Journal of Atmospheric and Solar-Terrestrial Physics*, vol. 108, pp. 77–90, 2014.

[43] S. Jin, G. Occhipinti, and R. Jin, "GNSS ionospheric seismology: Recent observation evidences and characteristics," *Earth-Science Reviews*, vol. 147, pp. 54–64, 2015.

[44] D. Marchetti, A. De Santis, S. Jin, S. A Campuzano, G. Cianchini, and A. Piscini, "Co-Seismic Magnetic Field Perturbations Detected by Swarm Three-Satellite Constellation," *Remote Sensing*, vol. 12, no. 7, p. 1166, 2020.

[45] P. Lognonné, R. Garcia, F. Crespon, G. Occhipinti, A. Kherani, and J. Artru-Lambin, "Seismic waves in the ionosphere," *Europhysics News*, vol. 37, no. 4, pp. 11–15, 2006.

[46] C. O. Hines, "Internal atmospheric gravity waves at ionospheric heights," *Canadian Journal of Physics*, vol. 38, no. 11, pp. 1441–1481, 1960.

[47] M. Hernández-Pajares, J. Juan, J. Sanz, and A. Aragón-Àngel, "Propagation of medium scale traveling ionospheric disturbances at different latitudes and solar cycle conditions," *Radio Science*, vol. 47, no. 6, 2012.

[48] M. Hernández-Pajares, P. Wielgosz, J. Paziewski, A. Krypiak-Gregorczyk, M. Krukowska, K. Stepniak, J. Kaplon, T. Hadas, K. Sosnica, J. Bosy *et al.*, "Direct MSTID mitigation in precise GPS processing," *Radio Science*, vol. 52, no. 3, pp. 321–337, 2017.

[49] H. Yang, E. Monte-Moreno, and M. Hernández-Pajares, "Multi-TID detection and characterization in a dense Global Navigation Satellite System receiver network," *Journal of Geophysical Research: Space Physics*, vol. 122, no. 9, pp. 9554–9575, 2017.

[50] F. J. Harris, "On the use of windows for harmonic analysis with the discrete Fourier transform," *Proceedings of the IEEE*, vol. 66, no. 1, pp. 51–83, 1978.

[51] H. Yang, E. Monte-Moreno, and M. Hernández-Pajares, "Detection and description of the different ionospheric disturbances that appeared during the solar eclipse of 21 august 2017," *Remote Sensing*, vol. 10, no. 11, p. 1710, 2018.

[52] A. K. Maurya, M. N. Shrivastava, and K. N. Kumar, "Ionospheric monitoring with the chilean gps eyeball during the south american total solar eclipse on 2nd july 2019," *Scientific reports*, vol. 10, no. 1, pp. 1–10, 2020.

[53] S. L. Vadas and E. Becker, "Numerical modeling of the generation of tertiary gravity waves in the mesosphere and thermosphere during strong mountain wave events over the southern andes," *Journal of Geophysical Research: Space Physics*, vol. 124, no. 9, pp. 7687–7718, 2019.

[54] E. Becker and S. L. Vadas, "Explicit global simulation of gravity waves in the thermosphere," *Journal of Geophysical Research: Space Physics*, vol. 125, no. 10, p. e2020JA028034, 2020.

[55] J. Kong, L. Shan, X. Yan, and Y. Wang, "Analysis of ionospheric disturbance response to the heavy rain event," *Remote Sensing*, vol. 14, no. 3, p. 510, 2022.

[56] A. B. A. F. P. R. E. S. U. Ziese, Markus; Rauthe-Schöch, "Gpcc full data daily version 2020 at 1.0°: Daily land-surface precipitation from rain-gauges built on gts-based and historic data," *Global Precipitation Climatology Centre (GPCC), DWD, Internet Publikation*, 2020.

[57] X. Meng, O. Verkhoglyadova, A. Komjathy, G. Savastano, and A. Mannucci, "Physics-based modeling of earthquake-induced ionospheric disturbances," *Journal of Geophysical Research: Space Physics*, vol. 123, no. 9, pp. 8021–8038, 2018.

[58] Japan World Data Center for Geomagnetism, "Geomagnetic Equatorial Dst Data," Available online: http://wdc.kugi.kyoto-u.ac.jp/dst_provisional/201612/index.html (accessed on 18 Jan. 2021), 2016.

[59] Geo Forschungs Zentrum (GFZ), Potsdam, "Geomagnetic Planetary kp Data," Available online: ftp://ftp.gfz-potsdam.de/pub/home/obs/kp-ap/wdc/kp1612.wdc (accessed on 18 Jan. 2021), 2016.

[60] U.S. NOAA Space Weather Prediction Center (SWPC), "GOES X-ray Flux Measurement," Available online: ftp://ftp.swpc.noaa.gov/pub/warehouse/2016/2016_plots/xray/20161217_xray.gif (accessed on 18 Jan. 2021), 2016.

[61] U.S. NOAA/NWS, National Tsunami Warning Center, "Tsunami maximum amplitude graph ," Available online: https://www.tsunami.gov/previous.events (accessed on 18 Jan. 2021), 2016.

[62] European Centre For Medium-Range Weather Forecasts, "ERA5 Reanalysis (0.25 Degree Latitude-Longitude Grid)," 2019. [Online]. Available: https://rda.ucar.edu/datasets/ds633.0/

[63] K. Heki, "Ionospheric electron enhancement preceding the 2011 tohoku-oki earthquake," *Geophysical Research Letters*, vol. 38, no. 17, 2011.

[64] S. A. Pulinets, A. Krankowski, M. Hernandez-Pajares, S. Marra, I. Cherniak, I. Zakharenkova, H. Rothkaehl, K. Kotulak, D. Davidenko, L. Blaszkiewicz *et al.*, "Ionosphere sounding for pre-seismic anomalies identification (inspire): Results of the project and perspectives for the short-term earthquake forecast," *Frontiers in Earth Science*, vol. 9, p. 131, 2021.

[65] R. Ikuta, T. Hisada, G. Karakama, and O. Kuwano, "Stochastic evaluation of pre-earthquake tec enhancements," *Journal of Geophysical Research: Space Physics*, vol. 125, no. 11, p. e2020JA027899, 2020.

Heng Yang received the Ph.D. degree in signal theory and processing from the Universitat Politècnica de Catalunya (UPC), Barcelona, Spain, in 2019. He is currently an Associate Professor with the School of Electronic Information and Engineering, Yangtze Normal University, Chongqing, China. He has been a Post-Doctoral Researcher with IonSAT, Department of Mathematics, UPC. He is working on the technologies of global navigation satellite system (GNSS) ionospheric sounding, including the computation of real-time global ionospheric maps, the detection of ionospheric perturbations, and relationship with natural events.

Manuel Hernández-Pajares is a Full Professor and the Head of the UPC-IonSAT Research Group, Universitat Politècnica de Catalunya, Barcelona, Spain. He has been working on global navigation satellite system (GNSS) since 1989, and in new algorithms for precise ionospheric sounding and navigation since 1994. He has been a Principal Investigator of more than three dozens of international scientific projects. He has published 125 articles in Q1 and Q2 peer-reviewed journals, with 7000 citations, h index of 39 and i10-index of 108 (February 2022). He has coauthored six patents, most of them international. He was the Chair of the International GNSS Service (IGS) Ionosphere WG from 2002 to 2007.

Wojciech Jarmołowski is an Assistant Professor at the Department of Geoengineering of the University of Warmia and Mazury in Olsztyn, Poland, where he received his PhD in physical geodesy. His research interests focus on geostatistical modeling of geophysical quantities (gravity, TEC), satellite altimetry and LEO mission data analysis, as well as GNSS geodetic and geophysical applications.

Paweł Wielgosz is a Full Professor at the Department of Geodesy of the University of Warmia and Mazury in Olsztyn, Poland, where he heads a research group on Advanced Methods for GNSS Data Processing. His research interests cover satellite navigation, precise positioning, and GNSS-based ionosphere and troposphere studies. He is the chair of the IAG Sub-Commission 4.4 "GNSS Integrity and Quality Control".

Sharon L. Vadas is a senior research scientist at NorthWest Research Associates. She received her bachelor degrees in physics and chemistry from the University of Rochester in 1987, then received her masters degree and PhD in physics from the University of Chicago in 1990 and 1993, respectively. Her research interest is focused on the theoretical study and modeling of atmospheric gravity waves in the Earth's atmosphere, with a special emphasis on comparison between models and data.

Oscar L. Colombo has worked on studies of space missions to map the gravity field of Earth and other bodies of the Solar System; on the precise determination of the orbits of artificial satellites, the modelling of forces acting on them in particular. He has also worked on: several altimetric satellite missions, including ICESat 2 now in progress, for mapping the ocean surface, the tides and to monitor the rise in sea level related to climate change, the corresponding changes in the volume of ice in the cryosphere; on techniques for the precise navigation of a variety of vehicles and for precise surveying using GPS, as well as kinematic methods for the precise determination of orbits of satellites using data from GPS receivers onboard the spacecraft. He is a Senior Visiting Scientist at NASA Goddard Space Flight Center, a member of the Institute of Navigation and a Fellow of the IAG.

Enrique Monte-Moreno received the degree in telecommunication engineering and the Ph.D. degree in digital signal processing from the Universitat Politècnica de Catalunya, Barcelona, Spain, in 1987 and 1992, respectively, and the degree in philosophy and the degree in mathematics from the Universidad Nacional de Educaciòn a Distancia, Madrid, Spain, in 2000 and 2010, respectively. He is an Associate Professor with the Department of Signal Theory and Communications, Universitat Politècnica de Catalunya. His research interests include digital signal processing, automatic speech recognition, global navigation satellite system (GNSS), machine learning applied to economics, medical topics, and the study of the ionosphere.

Alberto Garcia-Rigo is Ph.D. in Aerospace Science and Technology and Eng. Of Telecommunications by UPC (2012). He is an international expert on GNSS-based ionospheric determination, space weather and positioning, with particular focus on real-time/prediction operational systems. He is currently working at the Institute of Space Studies of Catalonia (IEEC) as Head of the Project Management Office, also contributing to its Knowledge Transfer Office (since September, 2018). He is Associate Editor of IEEE JSTARS (since December, 2019) and part of the Organising Committee of the ESA's 4th Symposium on Space Educational Activities (SSEA, 2022). He also currently chairs a Joint Working Group within the International Association of Geodesy (IAG) Global Geodetic Observing System (GGOS) program.

Victoria Graffigna received her bachelor degree in 2015 from Universidad Nacional de La Plata (UNLP), Argentina, and master degree in 2017, from Universitat Politècnica de Catalunya. Presently, she is a PhD candidate at UNLP, and the focus of her research lies on GNSS processing for recovering geophysical signals.

Anna Krypiak-Gregorczyk is an Assistant Professor at the Institute of Geodesy and Civil Engineering of the University of Warmia and Mazury in Olsztyn (UWM). Her research interests cover GNSS-based ionosphere study. She is the chair of IAG JWG 4.3.3 "Validation of VTEC models for high-precision and high resolution applications".

Beata Milanowska received her master's degree in satellite geodesy in 2019, and is a research assistant at the Department of Geodesy of the University of Warmia and Mazury in Olsztyn, Poland. Her research interests are ionospheric modeling and model evaluation. She is a member of IAG JWG 4.3.3 "Validation of VTEC models for high-precision and high resolution applications".

Pau Bofill-Soliguer Pau Bofill-Soliguer received a degree in telecommunication engineering and a Ph.D. degree in artificial intelligence by the Universitat Politècnica de Catalunya, Barcelona, Spain, in 1986 and 1997, respectively. His research interests are in signal separation, pattern learning, ecological economy and engineering education.

Germán Olivares-Pulido obtained his degree in Physics in 2000 (UAB) and his PhD degree in Physics in 2007 (UAB). Since 2010 he has been working on geodetic techniques for ionospheric sounding and ionospheric modeling for GNSS algorithms. From 2010 to 2013 he worked as an assistant researcher at the Group of Geophysics in Luxembourg working on Bayesian techniques for stochastic time series analysis. In 2014 he worked as a senior researcher at the UPC-IonSAT group, at Universitat Politècnica de Catalunya, working on ionospheric modeling for SBAS and first-principles ionospheric models. In 2015 he worked as senior researcher at the university of Warmia and Mazury in Poland, where he helped to develop a regional ionospheric model based on Voronoi tessellation for the LOFAR project. From 2016 to April 2019, he developed a 3D ionospheric model to support PPP-RTK at the Australian Bureau of Meteorology. In April 2019, he joined the Space Weather team at Spire as Senior Ionosphere Modeler. Since June 2021 he has worked as a senior researcher at the UPC-IonSAT group.

Qi Liu received his master's degree in Geodesy from University of Chinese Academy of Sciences (UCAS) in 2019. And he is currently a Ph.D. candidate of Universitat Politècnica de Catalunya (UPC). His research interests include GNSS-based ionospheric sounding, space weather monitoring and GNSS positioning.

Roger Haagmans received his masters in Geodetic Engineering at Delft University of Technology in the Netherlands in 1988, He continued first as researcher and later as assistant professor in geodesy at Delf University of Technolgy until 1999. In 2000 he became associate professor in geodesy and surveying at the Argicultural University of Norway. In 2001 he joined ESA as head of the Earth Surfaces and Interior Section in the Earth Observation Programmes Directorate and currently he is senior advisor in ESA.